Simplified impedance/frequency-response results for intrinsically conducting solids and liquids

J. Ross Macdonald*

Texas Instruments Incorporated, Dallas, Texas 75222
(Received 21 June 1974)

The small-signal ac response is considered of a system containing a single species of positive charge and a single species of negative charge. The charge carriers may be of many different types (ions, electrons, vacancies, etc.) and are assumed to have arbitrary mobilities and valences. Quite general boundary conditions are considered which encompass the range from complete blocking to zero blocking (infinite reaction rate at the electrodes) for positive and negative charges separately. The present paper deals primarily with approximations to an earlier exact solution of the problem which, in general, lead to an equivalent circuit made up of three parallel $R\,C$ combinations in series. The elements of one of these parallel circuits, associated only with bulk effects, are frequency independent, and those of another, which are associated with nonzero blocking, may often be well approximated as independent. The third $R\,C$ section arises from diffusion effects, involves frequency dependent elements, and exhibits approximate Warburg frequency response over a considerable frequency range. In general, Cole–Cole or Nyquist impedance plane plots show three connected arcs, two of which are frequently good semicircles. These arcs are directly associated with the three $R\,C$ sections. Under many conditions, only two of the three arcs may appear and melding of arcs into each other can also occur. Very simple, as well as less simple, approximations are developed for the impedances of the individual $R\,C$ sections as well as the over-all impedance of the system. The accuracy of these approximations is evaluated, and it is shown how they may be used in unambiguous cases to analyze frequency response data to yield estimates of mobilities, valences, electrode reaction rate parameters, and bulk charge concentrations. Surprisingly, it is found that for a certain mobility ratio range, the center arc, associated with electrode reactions, well approximates a depressed semicircle of the Cole–Cole relaxation time distribution type, yet no distribution of relaxation times is present. Further, in the completely blocking case, where the center approximate semicircle is not depressed but has an infinite radius, the lower frequency portion does not necessarily begin with a vertical segment as frequency decreases but may be curved away from vertical over a considerable frequency range. General impedance results for the present unsupported conduction situation are found to be quite different in some ways from those following from supported electrolyte treatments. Such treatments should thus not be used to analyze unsupported situations. Finally, it is found that the parallel capacitance of the system, which may be far greater than ordinary double layer values, can exhibit appreciable regions of ω^{-m} frequency response with $0 \leq m \leq 2$, and with $m = 0.5$, 1, 1.5, and 2 values especially prominent.

I. INTRODUCTION

In a previous paper,[1] an exact, closed-form solution was presented for the small-signal impedance of a two-electrode, intrinsic–extrinsic conduction system containing mobile positive and negative charge species of arbitrary valence numbers z_p and z_n, arbitrary mobilities, μ_p and μ_n, and quite general boundary condition parameters, r_p and r_n, themselves simply related to ordinary effective rate constants.[2] Because of its generality, this solution should often be useful in analyzing experimental impedance-frequency results for semiconductors and insulators, aqueous and other liquid electrolytes, solid electrolytes such as superionic conductors, and fused salts. But, because of the extreme complexity of the exact solution, which depends on seven parameters even in its normalized form, it has, thus far, only been explored in detail for an intrinsic conduction situation.[2] This exploration was based on accurate computer calculations of the consequences of the exact theory. Further, it should be mentioned that the exact theory is only applicable in the extrinsic case for full impurity dissociation.

Although numerous explicit formulas were given[2] for impedance and admittance components as functions of frequency in restricted frequency ranges, one particular approach toward unifying and simplifying the results was discovered and briefly mentioned in the previous paper.[2] It was based on the finding that in the most general situation three connected arcs appeared when the imaginary and real parts of the impedance were plotted parametrically in the impedance plane as circle diagrams or Cole–Cole plots.[3] Under favorable conditions the two highest frequency arcs were excellent semicircles with origins on the real axis, while the lowest frequency arc was a distorted semicircle, showing typical Warburg/diffusion type behavior.[2,4] In general, anywhere from one to three of these arcs could appear with or without appreciable melding of one arc into another.

The above results suggested that the total impedance of the system, Z_T, might be usefully represented by the sum of three separate impedances in series, each made up of a conductance and capacitance in parallel.[2] Let the impedances of the three parallel circuits, each representing one of the possible arcs, be $Z_1 = Y_1^{-1}$, $Z_2 = Y_2^{-1}$, and $Z_3 = Y_3^{-1}$, where Z_1 applies at the low end of the frequency spectrum and Z_3 at the high end. The arcs will be correspondingly identified: thus, arc 1 is the low-frequency one. Two equivalent forms of the exact equivalent circuit have already been discussed.[1,2] An alter-

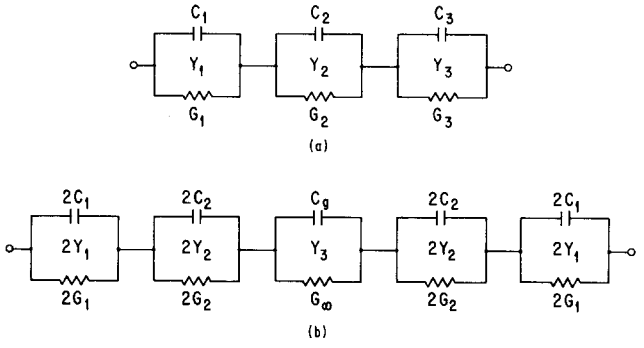

FIG. 1. (a) Possible exact series-parallel equivalent circuit. (b) Form of equivalent circuit for identical, plane-parallel electrodes.

nate form is that represented in Fig. 1(a). To the degree that arcs 2 and 3 are perfect semicircles, the capacitive and conductive elements of Y_2 and Y_3 are frequency independent. Further, Y_1 is essentially intensive (an interface quantity) when the frequency of the applied potential is not too low; Y_2 is intensive for all conditions of interest; and Y_3, which represents only the bulk properties of the basic material, is always extensive. The equivalent circuit can then be expanded to that of Fig. 1(b), applying for the situation of identical plane-parallel electrodes with identical boundary condition parameters.

The two parallel circuits on the left are thus associated with conditions at and within a Debye length or two of the left electrode except at such low frequencies that Y_1 becomes extensive. Here we have made the identification of the extensive Y_3 circuit elements as $C_3 \equiv C_g$, the geometric capacitance of the system in the absence of mobile charge, and $G_3 = G_\infty$, its bulk or solution conductance. These important frequency-independent quantities lead to the intensive time constant $\tau_D \equiv C_g/G_\infty \equiv C_g R_\infty$, the dielectric relaxation time. A symbol glossary is presented in the next section.

In the present work, the above series-parallel approach is further investigated, generalized, and evaluated for accuracy in a variety of situations of possible interest. Both simple and somewhat more complicated results useful in analyzing experiments are developed and compared with corresponding supported electrolyte expressions. All circuit elements will be taken as specific or unit area, quantities, and identical, plane-parallel electrodes and boundary conditions will usually be assumed. The results may be readily generalized to the situation of different electrodes and boundary conditions and to that where there is a single dominant working electrode with which is associated virtually all the intensive circuit elements (interface quantities) of importance. The results apply accurately in electrochemical situations only to the unsupported electrolyte case, but some of them apply, at least approximately, to the supported case as well. Further restrictions have been discussed earlier.[1,2] It is important to note that the present three arcs and corresponding three series-parallel circuits appear here for a single homogeneous material, not a three layer model, which can also lead to three parallel GC circuits in series.[5] The two situations should not be confused, and the present results should aid one to distinguish between them. Finally, although main emphasis here will be on intrinsic conduction situations, many of the formulas of the present work will be shown to apply to fully dissociated extrinsic conditions as well.

II. GLOSSARY OF SYMBOLS

A. Major subscripts

i	Designates an intrinsic or series "interface" quantity; also used as index with $i = n$ or p
n	Designates quantity associated with negative mobile charged species
p	Designates quantity associated with positive mobile charged species
N	Normalization of impedances and resistances with R_∞, of admittances and conductances with $G_\infty \equiv R_\infty^{-1}$, and of capacitances with C_g
P	A parallel quantity
S	A series quantity; also indicates a plateau region quantity
T	Stands for "total"
0	Designates either a static quantity or the zero-frequency limit of a frequency-dependent quantity
∞	The value of a quantity in the limit of high frequencies (i.e., $\Omega \gg 1$)

B. Major symbols in text

Numbers in parentheses indicate equations where the symbol is used or defined.

A	$(4G_{WPN}C_{WSN})^{-1/2}$; normalized Warburg parameter; (20)
A_0	Warburg parameter; (21)
C_d	Double layer capacitance; essentially MC_g in two-electrode situation
C_g	Geometric capacitance/unit area; $\epsilon/4\pi l$
C_i	"Interface" capacitance unit/area; the series capacitance associated with Z_i
C_{iS}	"Interface" capacitance/unit area in the plateau region
C_j	Capacitative components of Y_j; $j = 1, 2, 3$
C_P	Total parallel capacitance/unit area; associated with Y_T; Note: $C_{P0} \equiv C_0 \equiv C_{i0} + C_g$
C_{PS}	Total parallel plateau capacitance/unit area
C_{WS}	$(A\sqrt{\Omega})^{-1}C_g$; (A33)
D_i	Diffusion coefficient; for positive carriers $i = p$; for negative $i = n$
F	The Faraday
G_D	Frequency-independent parallel discharge conductance/unit area; $G_\infty - G_E$; (3); see Fig. 2
G_E	$(g_s G_\infty / g_p g_n) \equiv (G_\infty - G_D) \equiv R_E^{-1}$; see Fig. 2
G_j	Conductive components of Y_j; $j = 1, 2, 3$.
G_P	Total parallel conductance/unit area; associated with Y_T; Note: $G_{P0} \equiv G_D$; $G_{P\infty} \equiv G_\infty$
G_∞	Bulk conductance/unit area; R_∞^{-1}
L_D	Debye length in the present intrinsic case
M	$(l/2L_D)$
P_2	Value of $\mathrm{Re}(Z_T)$ at cusp between arcs 1 and 2; $(R_g + R_\infty)$; see Fig. 3 and Table I
P_I	Percent accuracy of approximation for $\mathrm{Im}(Z_{TN})$; (36)

P_R Percent accuracy of approximation for $\mathrm{Re}(Z_{TN})$; (35)
R Gas constant
R_{C1} Negative resistance in the Warburg region; (A26)
R_D G_D^{-1}; (3)
R_E Frequency-independent series resistance-unit area; G_E^{-1}; (4)
R_i "Interface" series resistance-unit area; associated with Z_i
R_R $(R_{C1}+P_2)$; (A36)
R_S $(R_{WS}+R_R)$; (A34)
R_{WS} $AR_\infty/\sqrt{\Omega}$; (A35)
R_θ Equilibrium charge transfer resistance-unit area; (10), (13), (14)
R_∞ G_∞^{-1}
T Absolute temperature
Y_i Z_i^{-1}
Y_j Z_j^{-1}
Y_T Total admittance/unit area of the system
Y_W Z_W^{-1}
Y_{12} Z_{12}^{-1}; (2)
Y_{1N1} Approximate expression for Y_{1N}; (A20) and Appendix E.
Y_{2N1} Approximate expression for Y_{2N}; (A14)
Z_i "Interface" impedance-unit area
Z_j Additive components of Z_T; $j=1,2,3$; (1)
Z_T Y_T^{-1}; (1)
Z_{TN1} Approximate expression for Z_{TN}; (A27)
Z_{TN2} Approximate expression for Z_{TN}; less accurate than Z_{TN1}; (34)
Z_W $A_0(1-i)/\sqrt{\omega}$; Warburg impedance; (18), (19)
Z_{12} $(Z_1+Z_2)\equiv(Z_T-Z_3)$
a $(\delta_p^2/\epsilon_p)+(\delta_n^2/\epsilon_n)$
b $\delta_n\delta_p/\epsilon_n\epsilon_p$
c $(\delta_n/\epsilon_n)-(\delta_p/\epsilon_p)$
d $(\delta_n/\epsilon_n)+(\delta_p/\epsilon_p)=a+b$
g_i $1+(r_i/2)$; $i=e$ $(r_n=r_p)$, n, or p
g_s $g_n\epsilon_p+g_p\epsilon_n$
g_z $g_n\delta_p+g_p\delta_n$
k_i Effective standard heterogeneous rate constants for the supported case; $i=n$ or p
l Distance of separation of plane, parallel electrodes
n Concentration of negative mobile charges
p Concentration of positive mobile charges; also $p^2\equiv 1+i\Omega$
r $M[\coth(M)]$
r_e Designation of common value of r_p and r_n when they are equal
r_n Dimensionless discharge parameter for negative charges
r_p Dimensionless discharge parameter for positive charges
s r_p/r_n; unity when $r_p=r_n=0$
t_j (γ_j-1); $j=1,2$; (A10)
z_n Valence number for negative mobile charges
z_p Valence number for positive mobile charges
Ω Normalized radial frequency; $\omega\tau_D$
Ω_j Value of Ω at peak of arc j; $j=1,2,3$
Ω_S $(a-1)^{-1}$
α Equilibrium transfer coefficient; also parameter in Cole–Cole dispersion formula
β Angle of approximate Warburg response line; (A38)
γ_j $(M\theta_j)\coth(M\theta_j)$; (A9)
δ_n $(1+\pi_z^{-1})^{-1}\equiv z_n/(z_n+z_p)$
δ_p $(1+\pi_z)^{-1}\equiv z_p/(z_n+z_p)$
δ_x δ_p for $\pi_m\ll 1$; δ_n for $\pi_m\gg 1$
ϵ Dielectric constant of the bulk material
ϵ_n $(1+\pi_m^{-1})^{-1}\equiv\mu_n/(\mu_n+\mu_p)$
ϵ_p $(1+\pi_m)^{-1}\equiv\mu_p/(\mu_n+\mu_p)$
η_1 The peak height of arc 1; see Fig. 3
θ_j Eigenvalues; $j=1,2$; (A1), (A2)
λ_1 The arc 1 length (R_D-P_2); see Fig. 3
μ_i Mobility; $i=n$ or p
ξ_i $(D_i/l)r_i$; $i=n$ or p; effective rate constants; (11), (12)
π_e Designation of common value of π_m and π_z when they are equal
π_m Mobility ratio; μ_n/μ_p
π_z Valence number ratio; z_n/z_p
ρ_2 Radius of arc 2; $R_\theta/2$; see Fig. 3 and Table I
τ_D Dielectric relaxation time; C_gR_∞
ω Radial frequency of the applied sinusoidal voltage

III. BACKGROUND

A normalized impedance situation is fully defined in the intrinsic conduction case by the following six parameters, $(r_p, r_n; \pi_m, \pi_z; 0, M)$ and Ω. Here $\pi_m\equiv\mu_n/\mu_p$; $\pi_z\equiv z_n/z_p$; $M\equiv l/2L_D$; and the normalized frequency is $\Omega\equiv\omega\tau_D$. The range of interest of Ω is $0\lesssim\Omega\lesssim 1$. In these expressions, l is the electrode separation, L_D the intrinsic Debye length, and ω the radial frequency. Electroneutrality holds in the bulk of the material when $M\gg 1$. When $r_p=r_n=0$, the electrodes are completely blocking for both mobile charge carriers. Alternatively, when $r_p=0$, $r_n=\infty$, the negative carrier is completely unblocked and reacts at an electrode with an infinite effective rate constant. It is important to note that because of symmetry if the quantities $(r_p, r_n; \pi_m, \pi_z; 0, M)$, which define a given situation, represent specific values, then the situation $(r_n, r_p; \pi_m^{-1}, \pi_z^{-1}; 0, M)$ is fully equivalent as far as its normalized total impedance Z_T/R_∞ is concerned.[1]

Let a subscript "N" denote normalization of impedances and resistances with R_∞, admittances and conductances with G_∞, and capacitances with C_g. Then we may write

$$Z_{TN}=Z_{1N}+Z_{2N}+Z_{3N}, \tag{1}$$

where Z_{TN} is the exact normalized impedance of the system. Since $C_{3N}\equiv C_g/C_g=1=G_{3N}=G_\infty/G_\infty$, one readily finds that $Y_{3N}\equiv(G_3+i\omega C_3)/G_\infty$ may be written as $Y_{3N}\equiv 1+i\Omega\equiv p^2$.

It only remains to obtain useful expressions for Y_{1N}

and Y_{2N}. Unfortunately, it is impractical to derive these in general from the exact solution, both because of its complexity and because the results would themselves be too complex to be very useful. Nevertheless, the general solution and its simple exact results in certain specific situations can be of great value in determining the general forms of Y_{1N} and Y_{2N} and limiting cases of these quantities. Beyond this, exact computer results can help one discover specific forms which jointly meet the goal of maximum useful simplicity married to adequate accuracy.

Let $(Z_{TN} - Z_{3N}) \equiv Z_{12N} \equiv (Z_{1N} + Z_{2N})$. The previous work then leads to the important quantity

$$Y_{12N} \equiv Z_{12N}^{-1} \equiv G_{12N} + i\Omega C_{12N} \equiv p^2[(p^2 R_{EN} - 1) + p^2 R_{EN}^2 Y_{iN}] . \quad (2)$$

When the quantity Y_{iN} is taken from the exact solution of the problem,[1] Y_{12N} may be obtained exactly as well. When Y_{1N} or Y_{2N} is infinite, Y_{12N} equals the noninfinite member of the pair. Here R_D and R_E are frequency-independent elements in the exact equivalent circuit[1,2]; in normalized form they are given by

$$R_{DN} \equiv G_{DN}^{-1} \equiv \{\epsilon_n[1 + (2/r_n)]^{-1} + \epsilon_p[1 + (2/r_p)]^{-1}\}^{-1} . \quad (3)$$

and

$$R_{EN} \equiv G_{EN}^{-1} \equiv \{\epsilon_n[1 + (r_n/2)]^{-1} + \epsilon_p[1 + (r_p/2)]^{-1}\}^{-1} . \quad (4)$$

In addition, $\epsilon_n \equiv (1 + \pi_m^{-1})^{-1} = \mu_n/(\mu_n + \mu_p)$, $\epsilon_p \equiv (1 + \pi_m)^{-1} = \mu_p/(\mu_n + \mu_p)$, and $(\epsilon_n + \epsilon_p) \equiv 1$. Note also that $(G_{EN} + G_{DN}) \equiv 1$.

The normalized admittance Y_{iN} is the only frequency dependent quantity in the exact theory and exact equivalent circuit,[1,2] two equivalent forms of which are shown in Fig. 2. The impedance of the circuit of Fig. 1(a) may be made identical to that of Fig. 2(a) and (b) when some

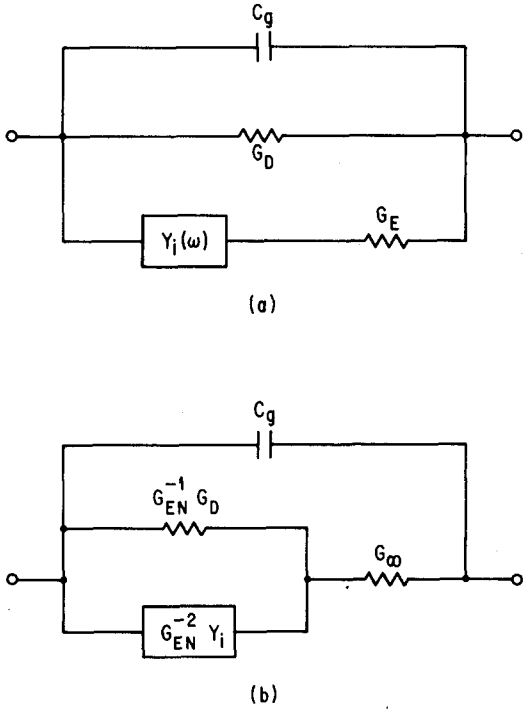

FIG. 2. (a) Exact equivalent circuit involving Y_i. (b) Alternate form of exact equivalent circuit.

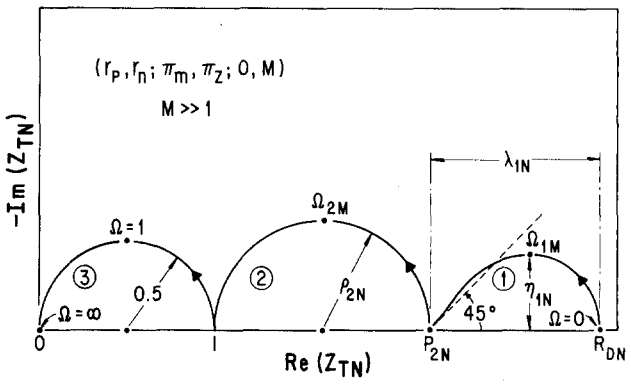

FIG. 3. General arcs and definition of quantities in the normalized impedance plane for $(r_p, r_n; \pi_m, \pi_z; 0, M)$.

frequency dependence is allowed for the Y_1 and Y_2 conductive and capacitative elements of Fig. 1(a). The inverse of Y_{iN} may be written $Z_{iN} \equiv R_{iN} + (i\Omega C_{iN})^{-1}$, where the series "interface" components R_i and C_i are both frequency dependent in general. If we write for the total normalized admittance of the system, $Y_{TN} \equiv Z_{TN}^{-1} \equiv G_{PN} + i\Omega C_{PN}$, then it follows that in the limit $\Omega \to 0$, which will be designated hereafter by a subscript zero, $G_{PN0} \equiv G_{DN}$ and $C_{PN0} \equiv 1 + C_{iN0} \equiv G_{DN}^2 + G_{EN}^2 C_{12N0}$. We may also write $Z_{TN0} \equiv G_{PN0}^{-1} = R_{DN} = Z_{1N0} + Z_{2N0} + Z_{3N0} = G_{1N0}^{-1} + G_{2N0}^{-1} + 1$. An exact expression for C_{iN0} is given in Appendix E.

IV. SOME APPROXIMATE RESULTS

A. Arcs

Let us first consider the simplest case: that where all arcs present are well defined and the cusps between them are sharp. Such behavior occurs when $M \gg 1$, so that there are many Debye lengths contained between the electrodes, and when $\Omega_{1M} \ll \Omega_{2M} \ll 1$, where these specific Ω's are defined in Fig. 3. Approximate expressions for the arcs and their underlying frequency response are then simplest and easiest to use to analyze experimental data. Some exact and less approximate results for various cases are discussed in the Appendix.

In general, three separate arcs can appear simultaneously, as illustrated in the diagrammatic normalized impedance plane representation of Fig. 3. The encircled numbers show the arc designations. In the present case, arcs 2 and 3 are good semicircles with centers on the real axis; arc 3 is fixed in size; and the sizes of arcs 1 and 2 may independently vary, making all sizes possible relative to arc 3. Note that with the present normalization the point 1 on the real axis corresponds to $\mathrm{Re}(Z_T) = R_\infty$. The point $\Omega = 1$ corresponds to $\omega = \tau_D^{-1}$, the frequency where the capacitative reactance of C_g equals R_∞. The general lengths: ρ_{2N}, λ_{1N}, and η_{1N}; points: P_{2N} and R_{DN}; and normalized frequencies at arc maxima on the imaginary axis: Ω_{2M} and Ω_{1M}; are defined as illustrated in Fig. 3. Note that $\lambda_{1N} \equiv R_{DN} - P_{2N}$.

Table I presents expressions for most of the above quantities for specific (r_p, r_n) choices of interest and increasing complexity. Note that when a length is zero the associated arc does not appear. The expressions for R_{DN} are exact here but those for the other quantities

TABLE I. Expressions for arc points and lengths for various values of r_p and r_n.

	Points		Lengths	
r_p, r_n	P_{2N}	R_{DN}	ρ_{2N}	λ_{1N}
$r_p = r_n \equiv r_e$	$1 + (2/r_e)$	$1 + (2/r_e)$	r_e^{-1}	0
$0, \infty$	1	ϵ_n^{-1}	0	π_m^{-1}
$0, r_n$	$1 + (2/\epsilon_n r_n)$	$\epsilon_n^{-1}[1 + (2/r_n)]$	$(\epsilon_n r_n)^{-1}$	π_m^{-1}
r_p, ∞	1	$\left(\frac{r_p + 2}{r_p + 2\epsilon_n}\right)$	0	$\frac{\pi_m^{-1}}{1 + (r_p/2\epsilon_n)}$
r_p, r_n	$1 + \left(\frac{2}{\epsilon_n r_n + \epsilon_p r_p}\right)$	R_{DN}	$(\epsilon_n r_n + \epsilon_p r_p)^{-1}$	$(R_{DN} - P_{2N})$

are only good approximations when cusps are well defined. In cases where arc 1 or 2 but not both appear and $\pi_m = \pi_g \equiv \pi_e$, exact expressions for Y_{1N} and Y_{2N} may be found (see Appendix B). Assessment of the accuracy of the present approximations will be given later. Figures 4–6 show idealized arc situations for some of the specific cases of Table I. Approximate equivalent circuits involving frequency-independent elements (except for Y_1) are also included in Figs. 4 and 5. A simple approximation for Y_{1N} is given later [Eq. (17)] and more accurate ones in Appendixes D and E.

B. Approximate components of Y_2

We have already seen that $Y_{3N} \equiv p^2 = 1 + i\Omega$, a simple Debye dispersion situation involving bulk properties only. Richer possibilities appear in Y_{2N} and Y_{1N}. In the present $r_n < \infty$, $M \gg 1$ case, we find that for $0 \leq \Omega \ll \Omega_S$

$$Y_{2N} \equiv G_{2N} + i\Omega C_{2N} \cong G_{2N0} + i\Omega C_{2N0} , \tag{5}$$

where the "0" subscript indicates the $\Omega \to 0$ limit as usual. The quantity Ω_S is approximately π_m for $\pi_m \ll 1$. A more general definition is given in Sec. V. This approximation of taking G_{2N} and C_{2N} essentially frequency independent is pertinent, of course, when arc 2 is a good semicircle, when $M \gg 1$, and for frequencies where $\Omega \ll 1$ and thus $p^2 \cong 1$. Exact results[1] for Y_{1N}, together with Eq. (2), then lead to the expressions

$$G_{2N0} \cong 0.5(\epsilon_n r_n + \epsilon_p r_p) \tag{6}$$

and

$$C_{2N0} \cong \tau + (\epsilon_n r_n + \epsilon_p r_p) , \tag{7}$$

where $\tau \equiv (M)\coth(M)$. Since $\tau \cong M$ here and $\rho_{2N} \equiv (\epsilon_n r_n + \epsilon_p r_p)^{-1}$ must be of the order of unity or greater for arc 2 to be comparable to or larger than arc 3, C_{2N0} may usually be well approximated as

$$C_{2N0} \cong M \tag{8}$$

when $M \gg 1$. Equations (6) and (7) are exact when $r_n = r_p \equiv r_e$. Finally one finds, when arc 2 appears in the region $0 < \Omega \ll \Omega_S$,

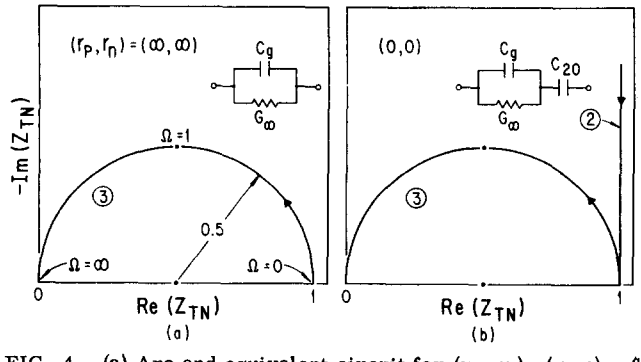

FIG. 4. (a) Arc and equivalent circuit for $(r_p, r_n) = (\infty, \infty)$. (b) Idealized arcs and approximate equivalent circuit for (0, 0).

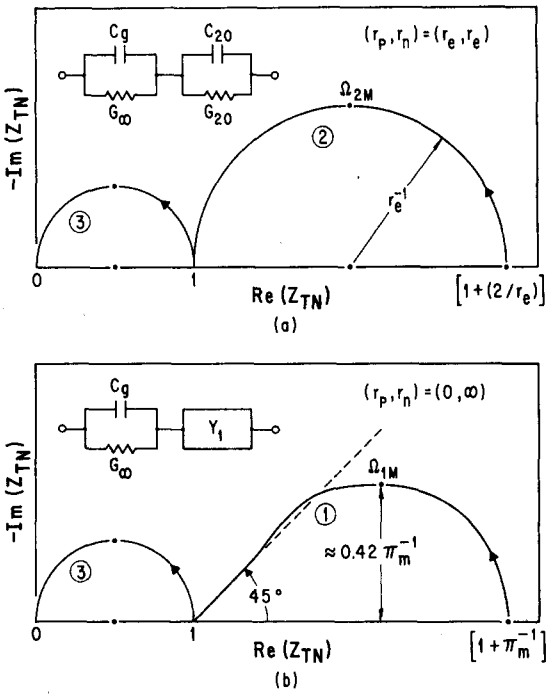

FIG. 5. Idealized arcs and approximate equivalent circuit for $(r_p, r_n) = (r_e, r_e)$. (b) Idealized arcs and equivalent circuit for $(0, \infty)$.

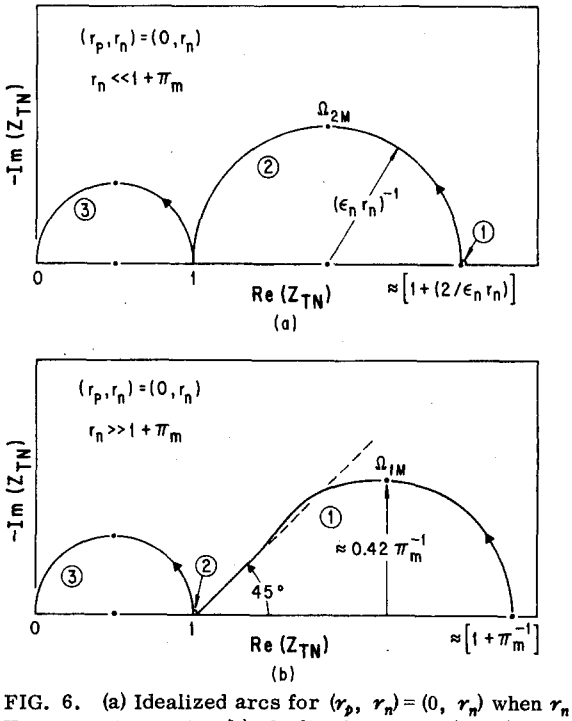

FIG. 6. (a) Idealized arcs for $(r_p, r_n) = (0, r_n)$ when $r_n \ll 1 + \pi_m$. Here $\pi_m \gg 1$, $r_n \sim 1$. (b) Idealized arcs for $(0, r_n)$ when $r_n \gg 1 + \pi_m$. Here $\pi_m \sim 1$, $r_n \gtrsim 10^2$.

$$\Omega_{2M} \cong G_{2N0}/C_{2N0} = (2\rho_2 C_{2N0})^{-1} \cong (\epsilon_n r_n + \epsilon_p r_p)/2M . \quad (9)$$

Clearly we must have $\Omega_{2M} \ll 1$.

Equation (8) leads to $C_{20} \equiv C_{2N0} C_g \cong MC_g = \epsilon/8\pi L_D$, where $C_g \equiv \epsilon/4\pi l$ and ϵ is the dielectric constant of the underlying bulk material. But $\epsilon/8\pi L_D$ is essentially just the expression for the unbiased double layer capacitance of two completely blocking ($r_p = r_n = 0$) double layers in series, one in the neighborhood of each electrode.[6] We thus see that in the context of the present approximation Z_2 is made up of just the blocking double layer capacitance, $C_d = C_{20}$, in parallel with a resistance

$$R_\theta = G_{2N0}^{-1} R_\infty = 2R_\infty/(\epsilon_n r_n + \epsilon_p r_p). \quad (10)$$

Since R_θ depends directly on the boundary parameters r_n and r_p and is infinite when they are both zero, it may be identified as an electrode reaction rate resistance, here expressed for two identical electrodes in series. Note that in unnormalized terms ρ_2 is just $R_\theta/2$ and P_2 is just $(R_\infty + R_\theta)$.

The above unnormalized results for arc 2 are formally exactly those found in the conventional supported electrolyte situation for a perfectly irreversible redox reaction.[7] There, a semicircle of radius $R_\theta/2$ begins at $(R_\infty + R_\theta)$ on the real axis and ends on the same axis at R_∞. (C_g is ignored in the conventional treatment, thus eliminating arc 3). But to what extent are the R_θ's appropriate in the two cases the same? Let us consider a single working electrode and introduce the unsupported-situation effective reaction rate constants[2]

$$\xi_n \equiv (D_n/l) r_n \quad (11)$$

and

$$\xi_p \equiv (D_p/l) r_p , \quad (12)$$

where D_n and D_p are the diffusion coefficients of the mobile charges. Since ξ_n and ξ_p are intensive, r_n and r_p are extensive.

For a single working electrode, designated with a superscript (1), the unsupported R_θ thus becomes

$$\begin{aligned} {}^{(1)}R_\theta &= (R_\infty/l)/(\epsilon_n D_n^{-1} \xi_n + \epsilon_p D_p^{-1} \xi_p) \\ &= (2RT/F^2)/(z_n n_i + z_p p_i)(z_n \xi_n + z_p \xi_p) \\ &= (RT/F^2)/(z_n^2 n_i + z_p^2 p_i)(\delta_n \xi_n + \delta_p \xi_p) \\ &= (RT/F^2)/(z_n^2 n_i \xi_n + z_p^2 p_i \xi_p) , \end{aligned} \quad (13)$$

where $R_\infty \equiv (l/F)[z_n \mu_n n_i + z_p \mu_p p_i]^{-1}$ has been used along with the electroneutrality condition $z_n n_i = z_p p_i$; n_i and p_i are the equilibrium bulk intrinsic-conduction charge concentrations; $\delta_n \equiv (1 + \pi_g^{-1})^{-1} = z_n/(z_n + z_p)$; $\delta_p \equiv (1 + \pi_g)^{-1} = z_p/(z_n + z_p)$; and $\delta_n + \delta_p \equiv 1$. In addition, the Einstein relation $D_i = (RT/Fz_i)\mu_i$ has been employed here with $i = n$ and p. The R_θ of Eq. (13) is clearly intensive; it differs somewhat from the corresponding R_{CS} resistance given earlier[2] because R_θ and R_{CS} appear in different equivalent circuits. When there are no reactions, $\xi_n = \xi_p = 0$ and $R_\theta = \infty$ in this blocking case. On the other hand, when either ξ_n or ξ_p approaches infinity, $R_\theta \sim 0$ and thus $Z_2 \sim 0$ as well. No double layer capacitance then appears in the present equivalent circuit. For $(r_p, r_n) = (0, r_n)$ and the typical values $T = 290$ K, $n_i = 10^{-3}M$, $z_n = 1$, and $\xi_n = 10^{-4}$ cm/sec, one finds ${}^{(1)}R_\theta \simeq 2.6 \times 10^3$ ohm-cm^2. For $D_n = 10^{-5}$ cm^2/sec and $l = 0.1$ cm, the r_n value corresponding to $\xi_n = 10^{-4}$ cm/sec is just unity.

The conventional supported R_θ is not usually given in the present case of possible simultaneous parallel reactions involving both the positive and negative charges ($0 \le \xi_n \le \infty$, $0 \le \xi_p \le \infty$). Generalization to this case has been given earlier[2]; the supported result is

$${}^{(1)}R_\theta = (RT/F^2)/(z_n^2 c_{ne} k_n + z_p^2 c_{pe} k_p) , \quad (14)$$

which may be directly compared to Eq. (13). Here k_n and k_p are the effective standard heterogeneous rate constants in the supported case and c_{ne} and c_{pe} are effective concentrations. If k_n is associated with a redox reaction, for example, c_{ne} is usually written as $c_O^\alpha c_R^{1-\alpha}$, where α is the equilibrium transfer coefficient and c_O and c_R are the concentrations of oxidizing and reducing species involved in the reaction. If we take the ξ's and the k's the same, (13) and (14) lead to the same resistance except for the apparent difference in the concentrations involved.

The quantities n_i and p_i appearing in (13) are bulk concentrations of charged species. On the other hand, the supported-electrolyte concentrations c_{ne} and c_{pe} usually involve the concentrations of both charged and uncharged species. But at the equilibrium potential, the point at which the present unsupported and supported treatments apply, $c_O = c_R \equiv c_e$ and $c_O^\alpha c_R^{1-\alpha} = c_{ne} = c_e$. This concentration is equivalent to n_i, for example. Since both the ξ's and k's are standard rate constants and thus account for both forward and reverse reactions, there is evidently no significant difference between the present unsupported R_θ and the conventional supported result at the equilibrium potential. The present results apply rigorously for very small ac perturbations around the equilibrium potential, especially when it coincides with the point of zero electrode charge in the electrochemical case, but they may also apply approximately in other regions where the current–voltage response is approximately linear[2] provided the rate constants are suitably interpreted.

C. Experimental analysis of arc 2 results

In unnormalized form Eq. (9) becomes

$$\omega_{2M} \cong (R_\theta C_d)^{-1} = (\epsilon_n r_n + \epsilon_p r_p) G_\infty/2C_d . \quad (15)$$

Since R_θ may be found from the P_2 intercept, C_d may then be obtained from the experimental value of ω_{2M}. Although R_∞ may be found from the left real-axis intercept of arc 2, one must extend measurements to at least $\Omega \gtrsim 0.1$ in order to determine C_g adequately. Then C_g, C_d, and ω_{2M} allow one to calculate M and L_D.

Figures 5(a) and 6(a) show two principal cases where only arcs 2 and 3 appear. While this is strictly true for the $r_n = r_p \equiv r_e$ case of Fig. 5(a), the condition $r_n \ll 1 + \pi_m$ applying in the $(0, r_n)$ case of Fig. 6(a) only ensures that arc 2 will always be far bigger than arc 1, not that arc 1 will be completely absent. Nevertheless, arc 1 may then not be experimentally distinguishable. To what degree can we then distinguish between these two similar

cases from experimental data? In the first case, $R_\theta = 2R_\infty/r_e$, while it is $2R_\infty/\epsilon_n r_n$ in the second. Let us now assume here that arc 1 is much smaller than arc 3 as well as arc 2. Then $\pi_m \gg 1$, $\epsilon_n \cong 1$, and thus $R_\theta \cong 2R_\infty/r_n$ in the case of Fig. 6(a). Unless vestiges of arc 1 can be identified in this case, there is no way to distinguish it from the first case to the present order of approximation. One then will not know whether R_θ involves r_e or r_n and thus whether the experimental situation involves equal r_n and r_p or $r_p = 0$, $0 < r_n < \infty$. Even the results of the exact theory will generally not allow distinction between the two cases except for data much more accurate than usually achievable.

Suppose that a good arc 2 semicircle, or even part of a semicircle, has been measured along with enough of arc 3 to yield C_g. Arc 1 may or may not be present. Assume that l and the electrode area are known and that both z_n and z_p are known as well, the usual experimental situation. It is of interest to summarize just what significant material parameters can then be calculated using the four arc 2 and 3 results: C_g, R_∞, R_θ, and ω_{2M}. Assume as usual that the circuit parameters are given per unit area. We may then calculate the estimates:

(a) $\epsilon = 4\pi l C_g$

(b) $C_d \cong (R_\theta \omega_{2M})^{-1}$

$M \cong C_{20}/C_g \cong C_d/C_g$

$L_D = l/2M$

$n_i = \epsilon R T \delta_n / 4\pi (F z_n L_D)^2$

$p_i = \pi_g n_i$

(c) $(\mu_n + \mu_p) = l/F z_n n_i R_\infty$

(d) $(z_n \xi_n + z_p \xi_p) \cong (2RT/F^2)(z_n n_i R_\theta)^{-1}$

$(\mu_n r_n + \mu_p r_p) \cong 2l/F z_n n_i R_\theta$

$(\epsilon_n r_n + \epsilon_p r_p) \cong 2R_\infty/R_\theta = 2R_{\theta N}^{-1}$.

From the four independent inputs, we calculate the four independent outputs ϵ, n_i and p_i, $(\mu_n + \mu_p)$, and $(z_n \xi_n + z_p \xi_p)$. It is clear that from these data alone we are unable to obtain estimates of μ_n, μ_p, ξ_n, and ξ_p separately.

To obtain μ_n and μ_p we must know π_m. Further,

$$(z_n \xi_n + z_p \xi_p) \equiv z_n \xi_n [1 + \pi_m^{-1}(r_p/r_n)]$$

when $z_n \xi_n \neq 0$. Thus to obtain ξ_n and $\xi_p \equiv (\pi_g/\pi_m)(r_p/r_n)\xi_n$, we must also know (r_p/r_n). In most cases of interest, this intensive quantity will be either unity or zero. If no trace of arc 1 appears at very low frequency the $r_p = r_n \equiv r_e$ assumption is indicated. Otherwise, one may either see vestiges of arc 1 or have information suggesting that r_p must be zero. Then in either of these cases ξ_n and ξ_p may be obtained. Even though π_m is not needed in the $(r_p/r_n) = 0$ case to obtain ξ_n, it is needed in the r_e case. Although as we shall shortly see, π_m may be readily obtained when arc 1 is significant, it can only be estimated in the r_e situation through the use of a higher-order approximation than that employed in the present section (see Appendix C).

Incidentally, although very little least squares analysis of complex data, such as impedance as a function of frequency, temperature, and/or dc bias, seems to have appeared in the literature, it is worth emphasizing that recently described methods of generalized least squares analysis[8] allow such data fitting to be carried out most expeditiously. This approach should be particularly appropriate in obtaining best parameter estimates from impedance or admittance data using one of the more accurate models, or impedance formulas, given in the Appendix.

D. Approximate components of Y_1

Simplification of the approximate expressions for Y_{1N} given in Eq. (A20) of Appendix D leads for $r_p \sim 0$ to the even more approximate result

$$Y_{1N} \equiv G_{1N} + i\Omega C_{1N} \cong [\pi_m (i\Omega b M^2)^{1/2} \coth (i\Omega b M^2)^{1/2}] \times [1 - s]^{-2}. \tag{16}$$

where $s \equiv r_p/r_n$, defined as unity when $r_p = r_n = 0$, and $b \equiv \delta_n \delta_p / \epsilon_n \epsilon_p$. The $(1 - s)^{-2}$ term in (16) is needed to make $Y_{1N} \to \infty$ when $r_p = r_n \equiv r_e$, a situation where arc 1 should not appear at all in the impedance plane plot.

It follows from Eq. (16) for the $(0, r_n)$ situation with $r_n > 0$ that $G_{1N0} \cong \pi_m$ and $C_{1N0} \cong b\pi_m M^2/3 = \delta_n \delta_p M^2/3\epsilon_p^2$, leading to extensive behavior for G_{10} and C_{10}. Equation (16) holds most accurately when $b\Omega \ll 1$. It leads to the arc 1 shape of Fig. 5(b). To this order of approximation, Y_{1N} is independent of $r_n (> 0)$ when $r_p = 0$; thus essentially the same shape appears for arc 1 in Fig. 6(b), where arc 2 is negligible. Note that when $\pi_m = \pi_z$, $b = 1$. Further when $\pi_z = 1$ and $\pi_m \ll 1$, $b \cong \pi_m^{-1}/4$ and $C_{1N0} \cong M^2/12$. For $M \gg 1$, C_{1N0} is then much larger than $C_{2N0} \cong M \cong C_{dN}$. The normalized admittance Y_{1N} approaches its low frequency limiting value when $\Omega < 2.5(bM^2)^{-1}$, and the maximum arc 1 height, $\eta_{1N} \cong 0.417\pi_m^{-1}$, is reached at $\Omega = \Omega_{1M} \cong 2.53(bM^2)^{-1}$. Note that the conditions $\Omega_{1M} \ll \Omega_{2M} \ll 1$ given earlier lead to the following conditions on M when the present approximate expressions for Ω_{1M} and Ω_{2M} are used: $M \gg (2\rho_{2N})^{-1}$ and $M \gg 5b^{-1}\rho_{2N}$. These inequalities only apply when $\rho_{2N} < \infty$.

Now when $\Omega > 10(bM^2)^{-1}$, $\coth(i\Omega b M^2)^{1/2} \simeq 1$ and for $s = 0$ one finds

$$Y_{1N} \cong (b\pi_m^2 M^2/2)^{1/2}(1 + i)\sqrt{\Omega}\,, \tag{17}$$

simple Warburg behavior. If we write for a Warburg impedance

$$Z_W \equiv A_0(1 - i)/\sqrt{\omega}\,, \tag{18}$$

and for Z_{WN}

$$Z_{WN} \equiv A(1 - i)/\sqrt{\Omega} \equiv R_{WSN} + (i\Omega C_{WSN})^{-1}\,, \tag{19}$$

then the present two-electrode results lead to

$$A \equiv (C_g/R_\infty)^{1/2} A_0 = (2\pi_m^2 b M^2)^{-1/2} = (\epsilon_p^2/M)(2\epsilon_n \epsilon_p \delta_n \delta_p)^{-1/2} \tag{20}$$

and

$$A_0 = \epsilon_p^2 [(2\sqrt{2}RT/F^2)(z_n n_i + z_p p_i)^{-1}] \times \{[(z_n D_n)^{-1} + (z_p D_p)^{-1}][z_n^{-1} + z_p^{-1}]\}^{1/2}\,. \tag{21}$$

Except for the presence of a factor of ϵ_p^2 here and a missing term involving r_p and r_n, these results for the Warburg parameters A and A_0 are exactly the same as those found previously.[2] The differences arise from the different equivalent circuits in which the parameters appear. Note that for $\pi_m \ll 1$ and $\pi_g = 1$, $A \cong (2/\pi_m M^2)^{1/2}$. The A_0 result is quite different from that found in the supported case, where Poisson's equation does not couple positive and negative charge motion appreciably. A detailed comparison has been given earlier[2] along with much examination and discussion of approximate Warburg response. Some deviations from exact Warburg behavior which follow from the present approach are discussed in Appendixes D and E.

E. Further experimental analysis

In order that the good separation shown in Fig. 2 between arcs 1 and 2 be maintained, it is necessary that $\Omega_{2M} \gg \Omega_{1M}$. This condition leads to $M \gg 5\epsilon_p/\delta_n\delta_p r_n$ for $r_p = 0$, which becomes $M \gg 20/r_n$ for $\pi_g = 1$ and $\pi_m \ll 1$ as well. Thus, in addition to the condition $M \gg 1$, r_n may not be too small if we wish to be able to distinguish arcs 1 and 2 adequately. Finally, comparison of Figs. 5(b) and 6(b) shows that the cases $r_p = 0$, $r_n = \infty$ and $r_p = 0$, $r_n \gg 1 + \pi_m$ cannot be well distinguished for the present order of approximation. When $\rho_{2N} \ll 0.5$, arc 2 will be indistinguishable, and it will not be possible to determine r_n or ξ_n. For $r_p = 0$ and $\pi_m \ll 1$, r_n can thus only be obtained from the present results when it falls in the range $5/\delta_n\delta_p M \ll r_n \lesssim 10\pi_m^{-1}$. This is probably somewhat too restrictive a condition on the low end, since even if arcs 1 and 2 overlap appreciably, they may still be adequately separated analytically in many cases if overlap is incomplete.

Let us continue to consider only the $(0, r_n)$ case for simplicity. If we now assume that ρ_{2N} and η_{1N} must both be 0.1 or greater to allow adequate observation of the associated arcs, we find $\pi_m \lesssim 4$ and $r_n \lesssim 10\epsilon_n^{-1}$ or $10(1 + \pi_m^{-1})$. Even though one may sometimes be able to measure with some accuracy impedance components whose magnitudes are less than $R_\infty/10$, it is clear that meaningful measurements in the arc 1 region will become very difficult to obtain when $\pi_m \gg 10$. Some other aspects of this problem have been discussed earlier.[2] Although measurements frequently cannot be extended to sufficiently low frequencies that all of arc 1 can be delineated, it is sufficient that enough of the bend away from Warburg behavior can be reached that extrapolation based on the known approximate shape of arc 1 will allow the height η_{1N} to be estimated. Then an estimate for π_m is $0.417\eta_{1N}^{-1} = 0.417 R_\infty/[-\mathrm{Im}(Z_T)_{\max 1}]$, where $-\mathrm{Im}(Z_T)_{\max 1}$ is the maximum height of arc 1 on the unnormalized impedance plane. Finally, this estimate of π_m may be used in the previous arc 2 equations along with arc 2 measurements to yield estimates of μ_n, μ_p, and ξ_n.

Since the sizes of arcs 1 and 2 depend on the separate factors π_m and r_n for $(0, r_n)$, one will have a certain amount of control of the relative sizes in this case because $r_n (\neq 0, \infty)$ is proportional to l. If arc 2, for example, is too small to measure accurately, its size may be increased by reducing l and thereby r_n, leading to a larger ρ_{2N}. Such variation should not, of course, have any effect on such intensive system parameters as ϵ, μ_n, μ_p, and ξ_n but it can help improve the accuracy with which they may be obtained.

The above conclusions apply when the arcs are given in normalized form. In unnormalized form, however, the sizes of all arcs are proportional to R_∞. Therefore, arcs 1 and 3 will increase in size proportional to l. On the other hand, ρ_2 is intensive since r_n and r_p are themselves directly proportional to l. Thus, ordinary unnormalized impedance plane plotting should lead to an arc 2 size almost entirely independent of l. As above, it can be made larger relative to the sizes of arcs 1 and 3 by decreasing l.

Although it is most convenient to determine π_m from the arc 1 height, η_{1N}, π_m may still be estimated when only the initial 45° straight-line portion of arc 1 is available and measurements cannot be extended down to Ω_{1M}. Let Ω_1 be a value of $\Omega (\gg \Omega_{1M})$ at a point in the straight line region. Then in this region $(Z_{TN})_{\Omega_1} \cong P_{2N} + (Z_{1N})_{\Omega_1}$. Therefore,

$$|Y_{1N}|_{\Omega_1} \cong |[(Z_{TN})_{\Omega_1} - P_{2N}]^{-1}| \cong \pi_m M \sqrt{b\Omega_1}, \tag{22}$$

where the last equation follows from Eq. (16) when $\Omega_1 b M^2 \gtrsim 10$.

Equation (22) readily leads to

$$\pi_m^{3/2} + \pi_m^{1/2} \cong (M^2 \delta_n \delta_p \Omega_1)^{-1/2} |Y_{1N}|_{\Omega_1} . \tag{23}$$

When R_∞ and C_g have been determined, one easily obtains Ω_1 and $|Y_{1N}|_{\Omega_1}$ from the experimental Z_T results. If it is assumed as usual that π_g is known, then $\delta_n\delta_p$ may be calculated. Finally, assume that M has been calculated from known quantities or estimated from an arc 2 experimental result such as a value of Ω_{2M}. Then the RHS of Eq. (23) is completely determined, and the cubic in $\pi_m^{1/2}$ may be solved to yield an estimate of π_m. Finally, previously presented expressions may be used to obtain μ_n, μ_p, and r_n estimates. A typical case where the above procedure is applicable is given by $(0, 80; 10^{-2}, 1; 0, 10^5)$ with $\Omega_{1M} \ll \Omega_1 \lesssim (100M)^{-1}$. A somewhat more accurate approach is outlined in Appendix E. The situation $0 < r_p < r_n < \infty$ will usually be considerably more complicated[1] and will not be discussed here.

It is worth noting that all formulas given in this paper and earlier[1,2] that involve only such π_m, π_g related quantities as ϵ_n, ϵ_p, δ_n, and δ_p, and quantities such as b derived from them, apply formally in the fully dissociated extrinsic conduction case as well as for intrinsic conduction.[1] Even those results which explicitly contain π_m and/or π_g can readily be generalized for the dissociated extrinsic situation by carrying out the transformations $\pi_m \to \pi_e$ and $\pi_g \to \pi_f$, where these quantities are defined in the full theory.[1] In the intrinsic case $\pi_m \equiv \pi_e$ and $\pi_g \equiv \pi_f$; for dissociated extrinsic conditions π_e and π_f (and thus ϵ_n, ϵ_p, δ_n, and δ_p) depend on the uncompensated impurity level and thus on the extrinsic parameter χ introduced in the earlier work.[1] The earlier work[1] is incorrect in implying that the theory holds for all extrinsic conditions. Its implicit assumption of homogeneous, immobile charged impurities limits its applica-

bility to the fully dissociated situation. Further, although dissociation of intrinsic neutral centers to give charged entities such as vacancies and interstitials determines the intrinsic charge level (n_i and p_i), the effect of recombination has otherwise been neglected.[1] Although some justification for such neglect has been given earlier,[2] it is hoped to include other effects of recombination exactly in future work.

V. TRANSITION REGION RESPONSE

Let the quantity a be defined as $[(\delta_p^2/\epsilon_p)+(\delta_n^2/\epsilon_n)]$. It turns out that $a=b$ when $\pi_g=1$. Further, when $\pi_g=\pi_m$, $a=b=1$. Finally, when $\pi_g=\pi_m^{-1}$, $b=1$ but $a\neq 1$ unless $\pi_g=1$ as well. We may now define the quantity Ω_s introduced in Sec. B as $(a-1)^{-1}$. Thus, when $(a-1)\Omega \ll 1$, Eq. (5) holds quite well. When $a=1$, Eq. (5) holds well over nearly the whole Ω range of interest, $0\leq\Omega\lesssim 1$. Since π_g is limited by physical considerations to the range $0.25\leq\pi_g\leq 4$, a and b cannot differ greatly, and we may usually approximate Ω_s by b^{-1} when $a\gg 1$.

On taking $\Omega_S=b^{-1}$ for simplicity, we find when $\Omega_{2M}\ll\Omega_S$ that for $r_n=r_p\equiv r_e$

$$(\Omega_{2M}/\Omega_S)\simeq b(r_e/2M). \tag{24}$$

Thus, it is necessary in this case that $(r_e/2M)\ll b^{-1}$. Note that symmetry ensures that Z_{TN} is the same in the $(r_e,\ r_e;\ \pi_m,\ \pi_g;\ 0,\ M)$ case for the two situations $\pi_m=B$, $\pi_g=D$ and $\pi_m=B^{-1}$, $\pi_g=D^{-1}$. The quantity $b\equiv(2+\pi_m+\pi_m^{-1})/(2+\pi_g+\pi_g^{-1})$ is $(2+B+B^{-1})/(2+D+D^{-1})$ for both these choices. Clearly π_m can be either too large or too small here for $(r_e/2M)\ll b^{-1}$ to hold adequately when r and M are fixed. It is this π_m transition region where Eq. (5) fails that we are particularly concerned with in this section.

Let us now consider the $r_p=0$, $0<r_n<\infty$ situation. Dominance of arc 2 as in Fig. 6(a) requires that $r_n\ll 1+\pi_m$, which may be satisfied for small enough r_n when $\pi_m\ll 1$. Let us, however, ask for the conditions that ensure that Z_{TN} is essentially the same for the situations $(r_e, r_e;\ B, D;\ 0,\ M)$, $(r_e, r_e;\ B^{-1}, D^{-1};\ 0,\ M)$, and $(0, r_n;\ B,\ D;\ 0,\ M)$, Figs. 5(a) and 6(a). It is thus necessary that $|Z_{1N}|\ll|Z_{2N}|$.

In the first two cases above, we have $R_{EN}=1+(r_e/2)\equiv g_e$, $R_{DN}=1+(2/r_e)$, and $G_{2N0}=r_e/2$, all independent of B and D. In the last case, on the other hand, one finds

$$R_{EN}=(1+B)g_n/(B+g_n), \tag{25}$$

$$R_{DN}=(1+B^{-1})[1+(2/r_n)], \tag{26}$$

and

$$G_{2N0}=Br_n/2(1+B), \tag{27}$$

where $g_n\equiv 1+(r_n/2)$. It is clear that these results well approximate those for the first two cases when $r_n\cong r_e$, $\pi_m=B\gg 1$, and $\pi_m=B\gg g_n$. These last two conditions may be combined into $\pi_m\gg 1+(r_n/2)$. Arc 2 is still dominant, and it turns out that Z_{TN} is very closely the same for the (r_e, r_e) and $(0, r_e)$ cases when $\pi_m\gg 1+(r_n/2)$. The results are quite different,[2] however, when $\pi_m\ll 1$.

Note that the $\pi_m\gg 1+(r_n/2)$ condition in the $(0, r_n=r_e)$ case ensures that the mobility of the discharging carrier is much greater than that of the blocked carrier. Then, arc 1 is negligible and arc 2 is essentially the same as that for the (r_e, r_e) case. As we have already noted, it may be virtually impossible to distinguish between the two cases unless additional physical information on the boundary processes is available. In the present $\pi_m\gg 1+(r_n/2)$ case, the dominant electrochemical step is the heterogeneous electrode reaction, which involves the most mobile charge carrier. On the other hand, when $r_n\gg 1+\pi_m$, and especially when $\pi_m\ll 1$, the dominant process contributing to the total impedance is diffusion to the electrode of the reacting charge carrier, which in the $\pi_m\ll 1$ case is much less mobile than the blocked carrier [see Fig. 6(b)]. As usual, the slowest process plays the major role in determining the impedance.

Now when Eq. (5) no longer holds well, Eq. (9) for Ω_{2M} is no longer a good approximation either. Let us see what happens under these conditions. Figure 7 shows some arc 2 results for various (π_m, π_g) values. Arc 3 has been omitted, as well as any vestiges of arc 1 for the two $(0, 1;\ 10^4,\ \pi_g;\ 0, 5\times10^4)$ cases shown. Note that although $(r_e/2M)\ll b^{-1}=1$ in the $(1, 1;\ 1,\ 1;\ 0, 5\times10^4)$ case, this inequality fails for the $\pi_m=10^4$ cases, where the (r_e, r_e) and $(0, r_e)$ results are essentially indistinguishable.

The most interesting result of Fig. 7 is the appearance of arcs with depressed centers, first distinguishable when π_m becomes appreciably larger than 100. Although the $\pi_m=1$ curve is essentially a perfect semicircle with its center on the real axis, in agreement with Eq. (5), the arcs for $\pi_m=10^4$ are both depressed and somewhat asymmetric. The broken line curves are symmetric depressed semicircles; some deviation from them occurs on the low-frequency side of the $\pi_m=10^4$ arcs. In many cases, these deviations might, however, be obscured by experimental error.

The listing in the figure shows the values of the Cole–Cole[3] α, related to the included angle $(\alpha\pi/2)$ defined below the real axis. Here α values have been derived from the best-fitting depressed semicircles, ignoring the low-frequency deviations. Clearly, for constant π_m, α is

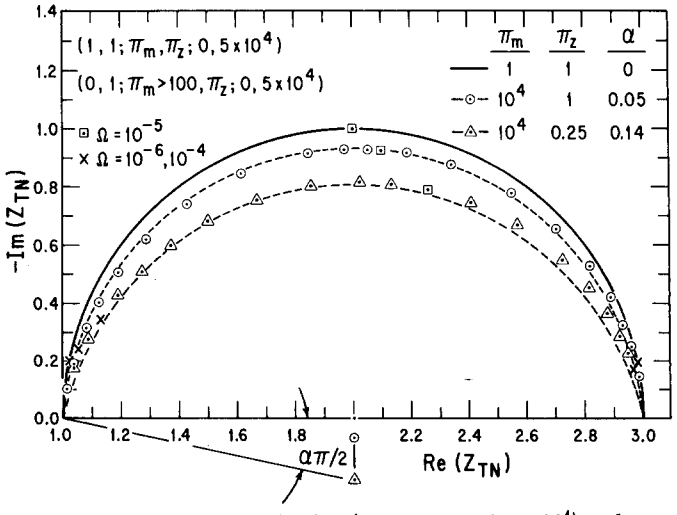

FIG. 7. Exact arc 2 results for $(1,1;\ \pi_m, \pi_g;\ 0, 5\times10^4)$ and $(0,1;\ \pi_m>100,\ \pi_g;\ 0,\ 5\times10^4)$ for various values of π_m and π_g.

larger than the $\pi_g = 1$ value when $\pi_g < 1$, and it approaches zero as π_g increases beyond unity. For $\pi_g = 1$, the maximum α of about 0.054 occurs at $\pi_m \equiv (\pi_m)_M$, approximately 4×10^4. As π_m increases beyond $(\pi_m)_M$, α approaches zero, reaching it by $\pi_m \sim 10^7$.

Depressed semicircles of the present type are usually described by the Cole–Cole dispersion formula,[3] which implies a wide distribution of relaxation times when $\alpha > 0$. Here such curves, or at least quite good approximations to them, occur without such a distribution but instead for a specific range of π_m values. For $(0, r_n; \pi_m, \pi_g; 0, M)$, this range clearly includes and is perhaps centered near $\pi_m \sim M$. This is then the center of the transition region, where $(\pi_m)_M \sim M$, and where maximum arc depression may be expected. Depressed arcs have been observed for such widely different materials as dielectrics,[3] biological substances,[9] and glass electrodes.[10] In many cases, especially the biological and glass areas just mentioned, it seems more likely that the present mechanism is operative rather than that there is a real distribution of relaxation times of the Cole–Cole type present.

The quantity $b(r_e/2M)$ is about 0.025 for the $\pi_m = 10^4$, $\pi_g = 1$ curve of Fig. 7. Equation (5) no longer holds well and usually the exact theory[1] must be used to analyze results in detail in this depressed-arc region. Approximately, however, one may estimate π_m from the amount of depression; but there is a chance of ambiguity in the result if shape alone is considered since curves with π_m both less and greater than $(\pi_m)_M$ have approximately the same shape when $\pi_g = 1$. There is some significant difference in shape, however, if it isn't obscured by experimental errors. When $\pi_g = 1$, Fig. 7 shows that points lie above the best-fitting depressed semicircle for $\Omega < \Omega_{2M}$ when $\pi_m < (\pi_m)_M$. When $\pi_m > (\pi_m)_M$, however, theoretical points lie above the depressed semicircle for $\Omega > \Omega_{2M}$. The arc associated with $(\pi_m)_M$ is thus essentially symmetric. It turns out, for example, that the arcs for $(\pi_m, \pi_g) = 10^4$, 1 and 10^5, 1 are almost mirror images of each other in the plane through the line $[\mathrm{Re}(Z_{TN}) = 2, -\mathrm{Im}(Z_{TN})$ arbitrary] and perpendicular to the paper.

To give some idea of frequency response, a few specific values are shown on the curves of Fig. 7. The $\Omega = 10^{-5}$ point corresponds to Ω_{2M} for $\pi_m = \pi_g = 1$; it is clearly not Ω_{2M} for the other values shown. Incidentally, the curves obtained for $\pi_m = 1$ and $0.25 \leq \pi_g \leq 4$ cannot be distinguished from those with $\pi_m = \pi_g = 1$ when plotted as in Fig. 7. This is not surprising since the RHS of Eq. (5) does not depend on π_g at all. When $\pi_g = 1$, the $\Omega = 10^{-5}$ point moves progressively toward larger $\mathrm{Re}(Z_{TN})$ values as π_m increases. By $\pi_m = 10^7$, it lies back on the $(\pi_m, \pi_g) = 1$ semicircle but with the coordinates $[\mathrm{Re}(Z_{TN}), -\mathrm{Im}(Z_{TN})] \cong 2.33, 0.94$ instead of 2, 1. Alternatively, when $\pi_m = 10^7$ and π_g varies, the point moves from 2.11, 0.99 at $\pi_g = 4$ down to 2.66, 0.74 at $\pi_g = 0.25$.

The change of curve shape with π_m variation when $\pi_g < 1$ is somewhat more complicated. Some typical results are shown in Fig. 8 for $\pi_g = 0.25$. No depressed semicircles have been drawn in here, and we see that there may be very appreciable deviations and asymmetry for $\pi_g = 0.25$. Clearly, for $\pi_m > 10^4$, the high frequency side of the arc approaches the limiting semicircle faster than the low frequency side. So much for the transition region, although the present few curves scarcely exhaust the different curve shape possibilities, especially when extrinsic conduction behavior is present.

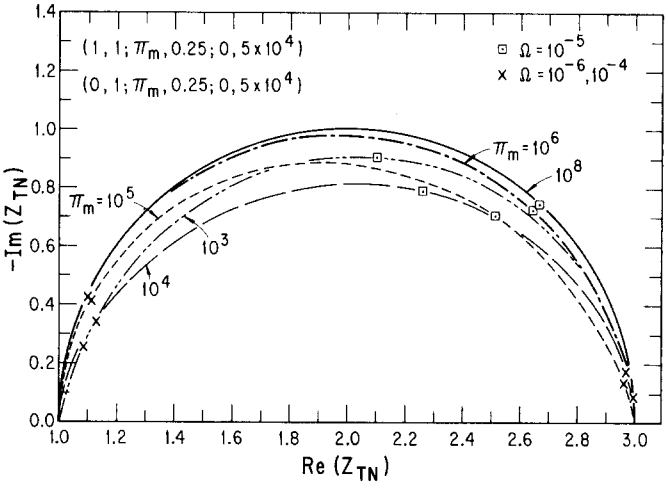

FIG. 8. Exact arc 2 results for (1, 1; π_m, 0.25; 0, 5×10^4) and (0, 1; π_m, 0.25; 0, 5×10^4) for various π_m results with $\pi_m \gg 1$.

VI. PLATEAU REGION RESPONSE

In the plateau region,[2] the smallest Ω value of interest is appreciably larger than Ω_S. Thus, the region to be examined is roughly bounded by $10b^{-1} \leq \Omega \lesssim 0.1$. It is therefore only of consequence when $b \gg 10$ and either $\pi_m \gg 1$ or $\pi_m \ll 1$. It is here called the plateau region because within it C_{iN} is virtually constant with a value C_{iSN} less than C_{iN0}. In the earlier work,[2] C_{iSN} was found to be essentially $g_e^{-2}(M\sqrt{\delta_p} - 1)$ for (r_e, r_e) and $g_p^{-2}(M\sqrt{\delta_p} - 1) = (M\sqrt{\delta_p} - 1)$ for $(0, r_n)$ when $\pi_m \ll 1$. Here $g_p \equiv 1 + (r_p/2)$. Arc 1 will then be very large. But the plateau region extends over an appreciable Ω span when $\pi_m \gg 1$ as well. In this situation, it turns out that $C_{iSN} \cong g_e^{-2}(M\sqrt{\delta_n} - 1)$ and $g_n^{-2}(M\sqrt{\delta_n} - 1)$ for the two cases above. For $\pi_m \gg 1$, arc 1 becomes negligible compared to arc 2, as we have seen. As discussed earlier,[2] the plateau region in C_{PN} is narrower than that which appears in C_{iN}. Generally, the range for the C_{PN} plateau, where $C_{PN} = C_{PSN}$, is approximately $10b^{-1} \lesssim \Omega < M^{-1}$. Thus, there is no appreciable plateau unless a is sufficiently large that $\pi_m^{\pm1} \gg M$ and conditions are thus beyond the $\pi_m \sim M$ transition region. Since the plateau region has already been considered[2] for the $(0, r_n)$ situation with $\pi_m \ll 1$, here main attention will be given to the $\pi_m \gg g_n$ case. Note that the shift from $\sqrt{\delta_p}$ to $\sqrt{\delta_n}$ in the above results arises because C_{iSN} essentially involves the real part of the eigenvalue θ_1 given in Eqs. (A5) and (A7) of the Appendix.

The quantities $M\sqrt{\delta_p} = l\sqrt{\delta_p}/2L_D$ and $M\sqrt{\delta_n} = l\sqrt{\delta_n}/2L_D$ are of especial interest. Using the definition of the intrinsic Debye length,[1] one readily finds that

$$L_D/\sqrt{\delta_p} \equiv L_{Dp} \equiv (\epsilon RT/4\pi F^2 z_p^2 p_i)^{1/2} \tag{28}$$

and

$$L_D/\sqrt{\delta_n} \equiv L_{Dn} \equiv (\epsilon RT/4\pi F^2 z_n^2 n_i)^{1/2} . \tag{29}$$

Here L_{Dp} and L_{Dn} are just the Debye lengths appropriate for positive charges only mobile and for negative charges only mobile, respectively. In the plateau frequency region, the mobility of the less mobile charge is so low relative to the relatively high frequency in this region that it can make no significant contribution[2] to C_i.

Figure 9(a), which follows directly from Fig. 2(a), shows the exact equivalent circuit applicable in the plateau region, where $C_i \cong C_{iS}$. But it turns out that R_i decreases rapidly as Ω increases in the plateau region. By $\Omega \gtrsim 25b^{-1}$, for example, R_{iN} is appreciably less than unity. Thus, in most of the plateau region, $R_{iN} \ll R_E$, and Fig. 9(b) then applies, a circuit made up entirely of frequency-independent elements. Finally, when $\pi_m \ll 1$, $R_E \cong R_\infty$ and $R_D \gg R_\infty$. Then R_D may be neglected and one obtains[2] Fig. 9(c).

Let us now see how an alternative series-parallel equivalent circuit of the Fig. 1(a) type can be obtained for the plateau region. It is clear that when the C_g of Fig. 2(b) is reconnected so that it is just in parallel with G_∞, one separates the total Z_T into two series-parallel circuits. The impedance of one of these circuits is just Z_3, and the other is, for $\Omega \ll 1$, nearly $Z_1 + Z_2 \equiv Z_{12} = Z_T - Z_1$. When $Z_1 = 0$, as in the $r_p = r_n \equiv r_e$ situation, Y_{2N} is just the Y_{12N} of Eq. (2). For this case, taking $R_{EN} = g_e$, one thus finds that for all Ω

$$Y_{2N} = Y_{12N} = p^2\left(p^2\frac{r_e}{2} + i\Omega + p^2 g_e^2 \frac{i\Omega C_{iN}}{1 + i\Omega C_{iN} R_{iN}}\right). \qquad (30)$$

The problem of obtaining a useful expression for Y_{2N} at least for $r_p = r_n \equiv r_e$ would then be solved if a simple expression for the frequency response of Z_{iN} were available. Further development of this possibility is carried out in the Appendix; here we need to consider only regions where C_{iN} is essentially frequency independent.

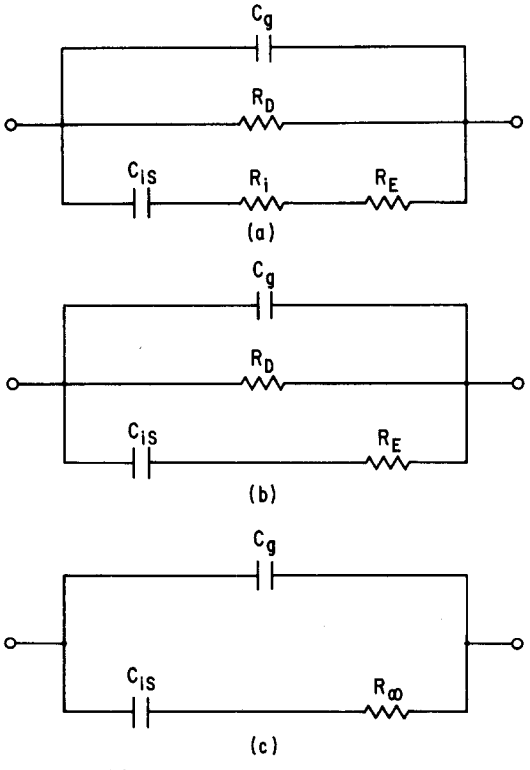

FIG. 9. (a) Exact equivalent circuit in plateau region (b) Usual approximate equivalent circuit over most of plateau region. (c) Approximate equivalent circuit for the plateau region when $\pi_m \ll 1$.

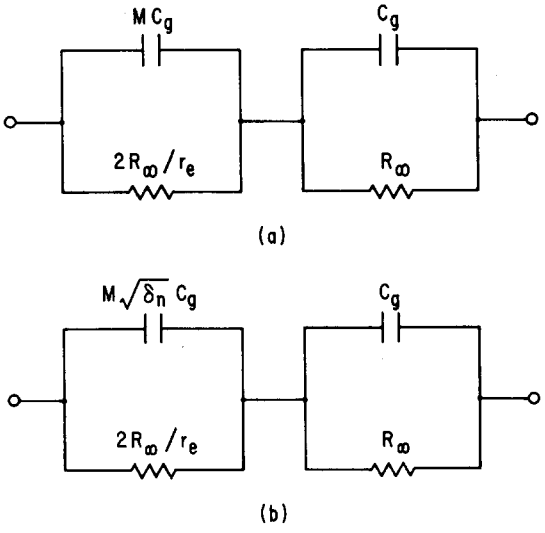

FIG. 10. (a) Approximate equivalent circuit for $(r_e,\ r_e;\ \pi_m,\ \pi_g;\ 0,\ M)$ and $(0,\ r_e;\ \pi_m \gg 1,\ \pi_g;\ 0,\ M)$ when $\Omega \ll \Omega_S = (a-1)^{-1}$. (b) Approximate equivalent circuit for same situations when $\Omega \gg \Omega_S$.

First notice that for $\Omega \to 0$ and with $C_{iN0} = g_e^{-2}(r-1)$, Y_{2N} from Eq. (30) approaches

$$Y_{2N0} = [(r_e/2) + i\Omega(r + r_e)], \qquad (31)$$

in agreement with Eqs. (5)–(7) for $r_p = r_n \equiv r_e$. Figure 10(a) shows the equivalent circuit applicable when $\Omega \ll \Omega_S$, taking $C_{2N0} \cong r \cong M$. The general relation $C_{12N0} \equiv R_{EN}^2 C_{iN0} + (2R_{EN} - 1)$, which applies here with $C_{2N0} = C_{12N0}$, is implicit in Eq. (2) and consistent with the term $G_{EN}^{-2} Y_i$ of Fig. 2(b). The corresponding G relation is $G_{12N0} \equiv (R_{EN} - 1) \equiv (R_{DN} - 1)^{-1} \equiv R_{EN} G_{DN}$.

Now it turns out that for the plateau region, where $\Omega \gg \Omega_S$, $(\Omega C_{iN} R_{iN})^2 \ll 1$ and C_{2SN} may be obtained to excellent approximation by replacing C_{iN0} in the above expression for C_{12N0} by C_{iSN}. Thus,

$$Y_{2N} \cong Y_{2SN} \cong p^2\{p^2[(r_e/2) + i\Omega M\sqrt{\delta_x}]\}$$
$$\cong [(r_e/2) + i\Omega M\sqrt{\delta_x}], \qquad (32)$$

where the second form applies when $\Omega \ll 1$ and $M \gg r_e$. Here δ_x is δ_p for $\pi_m \ll 1$ and δ_n for $\pi_m \gg 1$. The simple equivalent circuit corresponding to the second result in Eq. (32) is shown in Fig. 10(b) for $\pi_m \gg 1$. This circuit will usually be easier to apply than one of the circuits of Fig. 9.

Now in the $(0, r_n)$ case, we have seen that when $\pi_m \gg g_n$, $Z_{1N} \sim 0$ and may be neglected compared to Z_{2N}. Thus, in this situation the plateau admittance is also well approximated by Eq. (32) and Fig. 10(b) applies with r_e replaced by $\epsilon_n r_n \cong r_n$. Then in both the $r_p = r_n \equiv r_e$ and $(0, r_n)$ cases,

$$Y_{2N} \cong \{0.5(\epsilon_n r_n + \epsilon_p r_p) + i\Omega[M\sqrt{\delta_x} + (\epsilon_n r_n + \epsilon_p r_p)]\}. \qquad (33)$$

A somewhat more accurate expression is given in Eq.

TABLE II. Some exact and approximate results for the $(r_p, r_n; \pi_m, 1; 0, M)$ situation. $M = 5\times10^4$ for rows 1 through 12, and $M = 10^5/\sqrt{2}$ for rows 13–15.

					Z_{TN}		% Error Z_{TN1}		% Error Z_{TN2}	
Row	r_p	r_n	π_m	Ω	$\mathrm{Re}(Z_{TN})$	$-\mathrm{Im}(Z_{TN})$	P_R	P_I	P_R	P_I
1	1	1	1	10^{-6}	2.9802	0.19802	10^{-14}	-3×10^{-14}	9.8×10^{-6}	3.0×10^{-5}
				10^{-5}	1.99998	1.00003	10^{-14}	0	-1.9×10^{-8}	1.5×10^{-3}
2	0	2	1	10^{-6}	2.9911	0.21452	-1.1×10^{-1}	1.1	-1.1×10^{-1}	1.1
				10^{-5}	1.9977	1.0023	-3.3×10^{-1}	-2.2×10^{-1}	-3.4×10^{-1}	-2.2×10^{-1}
3	0	1.5	2	10^{-6}	2.9846	0.20629	-7.7×10^{-2}	7.8×10^{-1}	-7.7×10^{-2}	7.8×10^{-1}
				10^{-5}	1.9981	0.99976	-2.0×10^{-1}	-2.2×10^{-1}	-2.0×10^{-1}	-2.4×10^{-1}
4	0	3	0.5	10^{-6}	3.0024	0.22807	-1.5×10^{-1}	1.5	-1.5×10^{-1}	1.5
				10^{-5}	1.9981	1.0061	-5.2×10^{-1}	-2.3×10^{-1}	-5.1×10^{-1}	-2.4×10^{-1}
5	1	1	10	10^{-6}	2.9801	0.19783	-1.4×10^{-3}	-3.2×10^{-2}	-4.2×10^{-3}	-9.6×10^{-2}
				10^{-5}	2.0026	0.99746	4.3×10^{-2}	-8.5×10^{-2}	1.3×10^{-1}	-2.6×10^{-1}
6	0	1.1	10	10^{-6}	2.9798	0.19934	-3.6×10^{-2}	3.2×10^{-1}	-3.9×10^{-2}	2.5×10^{-1}
				10^{-5}	2.0013	0.99644	-3.1×10^{-2}	-2.2×10^{-1}	5.3×10^{-2}	-3.8×10^{-1}
7	0	11	10^{-1}	10^{-6}	3.0514	0.28700	-3.2×10^{-1}	2.7	-3.3×10^{-1}	2.7
				10^{-5}	2.0012	1.0218	-1.2	-3.5×10^{-1}	-1.2	-3.8×10^{-1}
8	1	1	10^2	10^{-6}	2.9797	0.19723	-5.7×10^{-3}	-1.3×10^{-1}	-1.7×10^{-2}	-4.0×10^{-1}
				10^{-5}	2.0107	0.98965	1.8×10^{-1}	-3.4×10^{-1}	5.3×10^{-1}	-1.0
9	0	1.01	10^2	10^{-6}	2.9794	0.19747	-1.7×10^{-2}	-2.6×10^{-2}	-2.8×10^{-2}	-2.9×10^{-1}
				10^{-5}	2.0103	0.98922	1.6×10^{-1}	-3.8×10^{-1}	5.1×10^{-1}	-1.1
10	0	101	10^{-2}	10^{-6}	3.2269	0.50225	-9.7×10^{-1}	4.8	-1.0	4.8
				10^{-5}	2.0093	1.0768	-3.9	-1.1	-3.9	-1.1
11	2	0.5	2	10^{-6}	2.9861	0.20518	-1.8	-25	-1.8	-25
				10^{-5}	2.0002	1.0019	-9.4×10^{-1}	-1.7	-9.4×10^{-1}	-1.7
12	0.5	2	0.5	10^{-6}	2.9861	0.20518	-3.0×10^{-1}	-3.7	-3.0	-3.7
				10^{-5}	2.0002	1.0019	-2.3×10^{-1}	-2.7×10^{-1}	-2.2×10^{-1}	-2.9×10^{-1}
13	1	1	10^8	10^{-6}	2.9793	0.19797	4.6×10^{-1}	74	-6.1×10^{-2}	-1.3×10^{-1}
				10^{-5}	1.99996	0.99955	-42	84	-1.0×10^{-3}	-9.8×10^{-2}
14	0	1	10^8	10^{-6}	2.9793	0.19797	4.6×10^{-1}	74	3.3	-1×10^4!
				10^{-5}	1.99996	0.99955	-42	84	5×10^{-2}	-200!
15	0	10^8	10^{-8}	10^{-6}	1.0997	19.9984	-14	89	-162	-1.0
				10^{-5}	1.00097	2.00001	-94	47	-99	-50

(A17). But arc 1 cannot generally be neglected when $\pi_m \ll 1$ for $(0, r_n)$. Therefore, in this case the full series-parallel circuit should be used for the plateau region with the usual Y_{1N}, arc 1, circuit added to that of Fig. 10(b), again with r_e replaced by $\epsilon_n r_n$, which is here essentially $\pi_m r_n$. Alternatively, Y_{1N} in the plateau region can be approximated by the expression for Y_{iSN} given in the Appendix, Eq. (A22).

For $r_n = r_p = r_e$, the arc 2 radius ρ_{2N} is r_e^{-1}, independent of π_m, and Ω_{2M} in the plateau region is approximately $r_e/2M\sqrt{\delta_x}$. If π_g is known, r_e and M may be readily obtained from ρ_{2N} and Ω_{2M} as in the $\Omega \ll \Omega_S$ case. Consider now the $(0, r_n)$ situation with the same ρ_{2N} as that for (r_e, r_e). It is then necessary that $\epsilon_n r_n = r_e$, or $r_n = (1+\pi_m^{-1})r_e$. To what degree can one distinguish between the two cases? When $\pi_m < 10$, even though the arc 2 sizes and shapes may be essentially identical, arc 1 will be present in the $(0, r_n)$ case and not in that with (r_e, r_e), thus allowing immediate discrimination between the cases. But when $\pi_m \gg g_n, r_n$ and r_e will be essentially identical and no significant arc 1 will appear for $(0, r_n)$. The quantity Ω_{2M} will also be very nearly $r_e/2M\sqrt{\delta_n}$ for both cases. Thus, discrimination will not be possible without additional information. Finally when π_m is completely unknown, unless M and π_g are known it will not even be possible to distinguish between the arc 2 shape associated with the $\Omega \ll \Omega_S$ condition and that present in the plateau region, $\Omega \gg \Omega_S$, when $\pi_m \gg g_n$ and all Ω's of interest are much less than unity.

VII. ACCURACY OF SOME APPROXIMATE RESULTS

Table II gives some numerical results for a variety of $(r_p, r_n; \pi_m, 1; 0, M)$ situations with $\rho_{2N} = 1$ and $\Omega_{2M} = 10^{-5}$ when these latter quantities are calculated from the pertinent formulas already given. We see that the actual exact results for $-\mathrm{Im}(Z_{TN})$ at $\Omega = \Omega_{2M}$ are very near the expected value of unity for rows 1–12. Also shown are values of the components of Z_{TN} at the low-frequency side of arc 2, $\Omega = 10^{-6}$. Very similar values for $-\mathrm{Im}(Z_{TN})$ are found at the other side, $\Omega = 10^{-4}$.

The remaining columns in Table II show the percentage errors arising in the various cases for the approximate expression for Z_{TN} given in the Appendix, Z_{TN1}, Eq.

(A27), and for the even more approximate expression Z_{TN2} made up of the foregoing results:

$$Z_{TN2} = Y_{1N2}^{-1} + Y_{2N2}^{-1} + Y_{3N}^{-1}, \tag{34}$$

with Y_{1N2} given by Eq. (16); Y_{2N2} by Eqs. (5)–(7) for the first twelve cases and Eq. (33) for the last three plateau-region cases; and $Y_{3N} = p^2 \equiv 1 + i\Omega$. In terms of Z_{TNj}, $j = 1$ or 2, P_R and P_I are

$$P_R \equiv 100\{[\mathrm{Re}(Z_{TN}) - \mathrm{Re}(Z_{TNj})]/\mathrm{Re}(Z_{TN})\} \tag{35}$$

and

$$P_I \equiv 100\{[\mathrm{Im}(Z_{TN}) - \mathrm{Im}(Z_{TNj})]/\mathrm{Im}(Z_{TN})\} . \tag{36}$$

In row 1, the P's for Z_{TN1} arise solely from roundoff since Z_{TN1} is exact for this situation. Although several situations will be noted where the errors in Z_{TN1} are appreciably smaller than those in Z_{TN2}, many times they are essentially equal. In such cases, the error observed arises principally from the way approximations for Z_{1N} and Z_{2N} are combined in forming an approximation for Z_{TN}, not from lesser inadequacies in the individual approximations.

The cases of rows 1–12 are just a few of the many situations which can lead quite accurately to $\rho_{2N} = 1$ and $\Omega_{2M} = 10^{-5}$. The exceedingly close similarity of most of these results will make it exceptionally difficult to discriminate between them. Since in several cases the numerical results at given Ω are closer together than the errors in Z_{TN1}, curve fitting using the exact expression for Z_{TN} will be necessary as well as exceptionally accurate experimental results in order to allow discrimination. Of course, outside the arc 2 region examined here, discrimination will usually be possible between such cases as $r_p = r_n = \pi_m = 1$ and $r_p = 0, r_n = 2, \pi_m = 1$ because of the appearance of some arc 1 behavior in the $r_p = 0$ case which is absent in the $r_p = r_n = r_e$ case. Discrimination between such cases as $r_p = r_n = \pi_m = 1$ and $r_p = r_n = 1$, $\pi_m = 10$ will be virtually impossible, however. Since $r_p = r_n$ is a more unlikely situation than $r_p \neq r_n$ or $r_p = 0$, $r_n \neq 0$, the need for such discrimination may not often arise, however.

Rows 7 and 10 show that as π_m becomes small, even though the desired values of ρ_{2N} and Ω_{2M} may be maintained by the proper choice of r_n, Z_{TN} will begin to be appreciably different away from Ω_{2M}. By symmetry, the exact results of rows 11 and 12 must be identical as shown. Note, however, that the Z_{TN1} results are appreciably more accurate for $(r_p, r_n) = 0.5, 2$ than for 2, 0.5. This happens because the expression for Z_{1N} entering Z_{TN1} has been optimized for (r_p, r_n) with $r_p \ll r_n$ rather than with $r_p > r_n$. Modification of this Z_{1N} approximation to make it show the symmetry of the exact solution would have made the expression given in the Appendix considerably more complicated. Such modification is unnecessary since the symmetry relation may be used to change any $r_p > r_n$ case into a $r_p < r_n$ case.

The final three rows of the Table show plateau cases. As expected, the errors of Z_{TN1} are large here. On the other hand, the Z_{TN2} expression appropriate for the plateau region has been used here, and the row 13 Z_{TN2} errors are small. The corresponding errors for row 14 are far from small, however. In this case the contribution to Z_{TN} from Z_{1N2} should have been negligible but was not. In $r_n \ll 1 + \pi_m$ plateau cases with $\pi_m \gg M$, one must clearly omit all Z_{1N} contributions. Row 15 shows that when $\pi_m \ll M^{-1}$, arc 1 plays a large role compared to arc 2 and the desired values of ρ_{2N} and Ω_{2M} are not obtained.

VIII. SOME IMPORTANT CURVE SHAPES

In the original paper in this series,[1] numerous curves were presented of the dependence of R_{iN0} and C_{iN0} on the parameters of the situation: $M, r_n, r_p, \pi_m, \pi_s$, and temperature. In the second paper,[2] many computer-calculated curves of C_{PN} and G_{PN} *versus* frequency and normalized impedance plane plots (such as Fig. 3) were included, again for various values of the input parameters. The exact curves of the present paper help fill in response possibilities not adequately covered by the previous work. A few important further responses of this kind are discussed in the present section.

Figure 11 shows some C_{PN} frequency response curves. Note that for $\pi_m^{\pm 1} \gg 1$, three different dispersion regions (associated with Z_{1N}, Z_{2N}, and Z_{3N}) appear in C_{PN} results when $r_n < \infty$. From right to left, the first rise is associated with the final bulk single-time-constant dispersion (Z_{3N}) and leads to the plateau region (here appearing at $10^{-7} \lesssim \Omega \lesssim 10^{-4}$). The second small rise, in the region of $\Omega \sim 10^{-8}$ to 10^{-9}, carries C_{PN} up to approximately the ordinary double layer value of M, and the final rise, whose onset clearly depends appreciably on the magnitude of r_n, carries C_{PN} to $C_{PN0} \equiv 1 + C_{iN0}$. For $\pi_m = 10^{-8}$, only the $r_n = \infty$ curve shows an appreciable region of slope -0.5, Warburg frequency response. It is important to point out that for $2 \lesssim r_n \lesssim 200$, appreciable regions with a slope of -1 appear. Such ω^{-1} frequency response has often been observed for various solids. The important implications of the result that C_{PN0} is asymptotically proportional to M^2 for $M \gg 1$, not M, so that C_{PN0} may be very large indeed, have been discussed earlier.[1,2]

The impedance levels which appear for the $\pi_m = 10^{-8}$

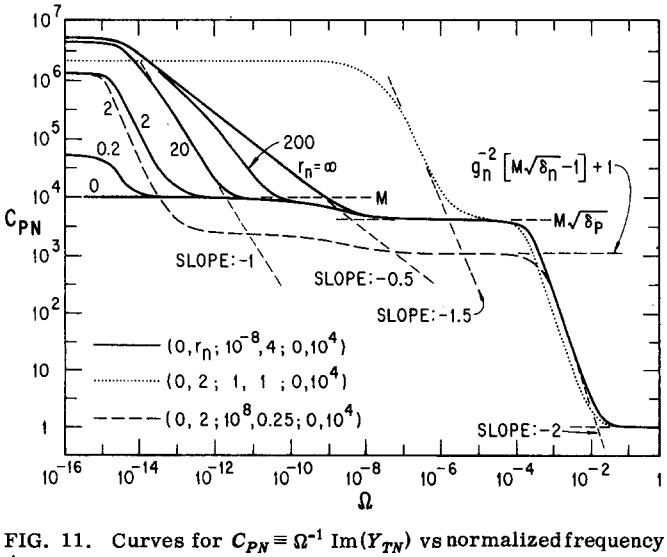

FIG. 11. Curves for $C_{PN} \equiv \Omega^{-1}\,\mathrm{Im}(Y_{TN})$ vs normalized frequency Ω for several situations.

TABLE III. Values of impedance components for $(0,2;\ \pi_m,\ \pi_g;\ 0,\ 10^4)$.

			$\Omega = 10^{-10}$		
π_m, π_g	R_{DN}	C_{PN0}	$\mathrm{Re}(Z_{TN})$	$-\mathrm{Im}(Z_{TN})$	C_{PN}
10^{-8}, 4	2×10^8	1.337×10^6	1.13×10^5	1.11×10^6	8888.6
1, 1	4	2.089×10^6	3.99999	3.34×10^{-3}	2.089×10^6
10^8, 0.25	2	1.341×10^6	2	8.93×10^{-7}	2232.9

curves are very high and hence relatively easy to observe. Thus for $(0,2;\ 10^{-8},\ 4;\ 0,10^4)$ at $\Omega = 10^{-14}$, $Z_{TN} \cong (1.17 - 0.189i)\times10^8$. At $\Omega = 10^{-8}$, $Z_{TN} \cong (3.31 - 19.1i)\times10^3$. On the other hand, the situation is quite different for the $\pi_m = 10^8$ curve. For $(0,2;10^8,\ 0.25;\ 0,10^4)$, $Z_{TN} \cong (2 - 1.89\times10^{-9}i)$ at $\Omega = 10^{-14}$, $(2 - 5.08\times10^{-5}i)$ at $\Omega = 10^{-8}$, and $(1.998 - 4.47\times10^{-2}i)$ at 10^{-5}. Table III shows some results for $\Omega = 10^{-10}$. In these frequency ranges $\mathrm{Re}(Z_T)$ dominates, and it will usually be difficult to measure $\mathrm{Im}(Z_T)$ much below perhaps $\Omega = 10^{-6}$. Thus, although the C_{PN} curve is given for smaller Ω in Fig. 11, it will not be measurable. This result is consistent with that of Fig. 6(a) which shows the effect of Z_{1N} to be negligible for $r_n \ll 1 + \pi_m$.

The curves indicate that the lower limit of the plateau region is between $10b^{-1}$ and b^{-1}. Here $b^{-1} \sim 6\times10^{-8}$ for both the two $r_n = 2$ curves with $\pi_m = 10^{-8}$ and 10^8. Thus, the lower frequency parts of the curves will appear at lower and lower frequencies the larger b. For $\pi_m \to 0$ and for $\pi_m \to \infty$, one will therefore again find the plateau region extending all the way down to $\Omega = \epsilon$, with $\epsilon \to 0$. Under such conditions, only one species of charge is effectively mobile, and C_{PN} cannot exceed C_{PSN}.

The normalized impedance plane results of Fig. 12 are interesting because such shapes are frequently found experimentally[11–14] and also because very nearly the same sort of results appear in theoretical treatments of the supported electrolyte situation.[7,15] Note that the curves as shown do not extend far enough to the right to include the low frequency limiting region of arc 1, associated with Z_{1N}. It is interesting that the curve of Fig. 1(b) of Ref. 14 for the superionic solid electrolyte Ag_4RbI_5 is very close in shape to that for $M = 10^3$ in Fig. 12. The authors of Ref. 14 were unable, however, to obtain results in the high-frequency region of arc 3.

Although the shapes of theoretical impedance plane curves for the supported electrolyte case[7,15] are very similar to those of Fig. 12, their dependence on M and L_D seems considerably different. Here the cusp between arcs 1 and 2 becomes sharper and sharper the larger M, or the smaller L_D. But Sluyters[15] gives supported curves which show sharper and sharper cusps as the double layer capacitance C_d decreases (L_D increases). The intercept of the Warburg 45° line extended back to the real axis is also somewhat different in the two cases.[7] These results suggest that it is quite important to use theoretical results for the unsupported situation[1,2] rather than supported-electrolyte theory in cases where the unsupported situation is likely. It is quite probable that the unsupported assumption will be applicable for many superionic conductors, fused salts; and intrinsic-defect-conduction single crystals[16] at temperatures where electron–hole conduction is negligible.

The dependence of some of the present curves on l variation is also of some interest. First note that Ω and MC_g are independent of l. When the C_{PN} of Fig. 11 is changed to $C_P \equiv C_{PN}C_g$, an increase in l (or in M arising from the l increase) will make no significant change in C_P in the plateau frequency region or above when $M \gg 1$. Even in the $C_P \simeq MC_g$ region, when it appears, l variation will have little or no effect on C_P. But whenever $C_P > MC_g$, an increase in l will tend to increase C_P, since $C_{P0} \propto M^2C_g \propto l$. These regions of the graph thus depend strongly on l, and the results are extensive, not intensive there. Since the normalization of Z_{TN} in Fig. 12 involves $R_\infty \propto l$, the scales of both axes change together when l changes. It has already been mentioned that when unnormalized impedance plots are considered, the sizes of arcs 1 and 3 will be directly proportional to l, but the arc 2 size is independent of l. Since arc 2 is associated with electrode reactions, it should indeed be intensive. It is, of course, in the intensive plateau region of Fig. 11 that arc 2 makes its contribution to C_{PN}.

The region near the cusp between arc 3 and arc 2 (or arc 1 if 2 is missing) is of particular interest. Frequently, frequency response measurements cannot be readily extended to sufficiently low frequencies that all of arcs 2 and 1 can be covered. Then, one must depend on the limited measurement region available in order to try to reach sensible conclusions about what happens in the experiment. Separation of the effects of electrode reactions and diffusion is particularly difficult when these effects overlap in frequency, as they do somewhat in Fig. 12 for $M \lesssim 10^4$. But the ambiguity can be much greater.

When the frequency region covered between the end of arc 3 and the lowest frequency measurable is quite limited, it may be exceedingly difficult to tell whether the situation being investigated involves $(r_p, r_n) = (0, 0)$, (r_e, r_e), or $(0, r_n)$. Figure 13 shows some results for $(0, 2\times10^4;\ \pi_m,\ 1;\ 0, 10^4)$. Although we have $0 < r_n < \infty$

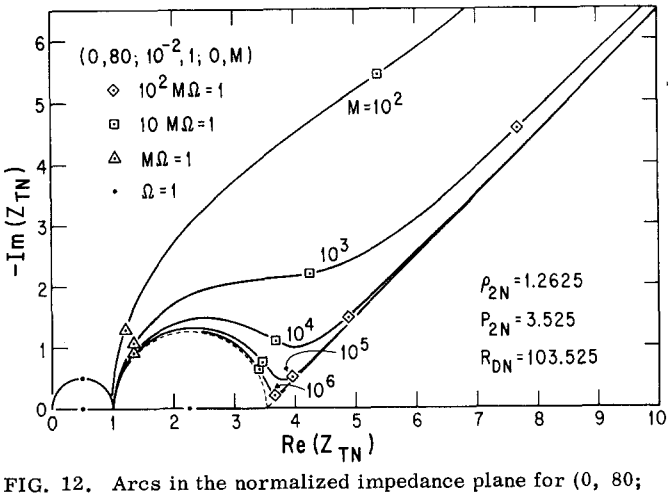

FIG. 12. Arcs in the normalized impedance plane for (0, 80; 10^{-2}, 1; 0, M) showing approximate Warburg-response lines at the right. The figure does not extend to low enough frequencies to show all of arc 1.

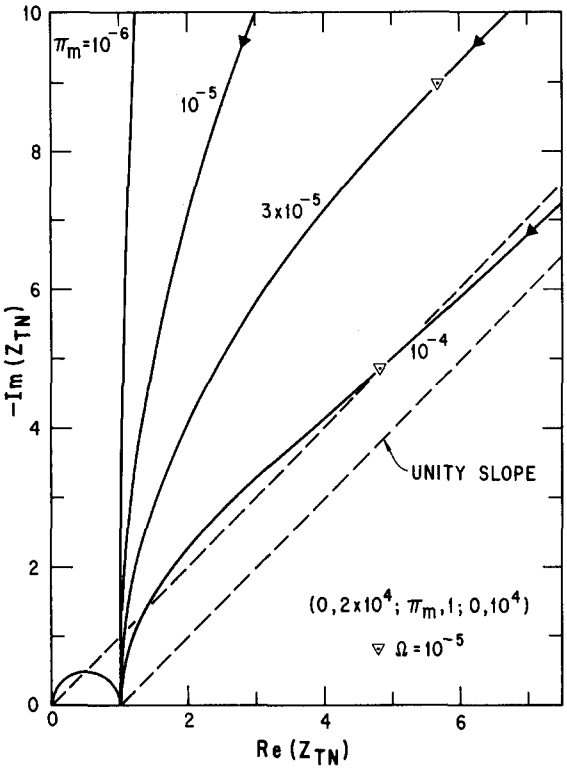

FIG. 13. Normalized impedance plane results for $(0,2\times10^4;\ \pi_m,\ 1;\ 0,\ 10^4)$ and $\pi_m \leq M^{-1}$. Arc 1 closure not shown.

here, the $\pi_m \ll 1$ curves shown are not good approximations over very much of their extent to the initial parts of semicircles in the region $\mathrm{Re}(Z_{TN}) \gtrsim 1$. The effect of r_n here is to change the curve shape somewhat and slow the eventual approach to Warburg behavior but not to yield any distinguishable arc 2 semicircle. Here, in fact, all curves eventually become asymptotic to the dashed Warburg line through the point $-\mathrm{Im}(Z_{TN})=0$, $\mathrm{Re}(Z_{TN})=1$ before finally approaching the real axis as $\Omega \to 0$.

Armstrong *et al.* have suggested[17] that even in a completely blocking (0, 0) situation, where one would ordinarily expect a vertical rise, as in Fig. 4(b), the rise may be curved over, as in the curves of Fig. 13, because of the presence of electrode surface roughness.[18] Here, where we deal with smooth electrodes, such curvature can appear because blocking is not complete and some electrode reaction occurs at the electrode. One may possibly be able to distinguish between the two causes of curvature by varying the roughness of the electrode surface. But there will usually be no guarantee that going from a very smooth surface to a rougher one will not itself appreciably increase the probability of an electrode reaction. A rough surface will have asperities where the electric field will be far higher than that for a smooth surface. Such a high field will itself most probably enhance electron transfer at the electrode. Therefore, in practice it may be difficult to distinguish between a rough (0, 0) surface and a rough $(0, r_n)$ surface.

But Fig. 14 shows that the situation is even more uncertain. Here we see what happens for a theoretical smooth (0, 0) surface when the mobility ratio is far different from unity. Again the low frequency curves are not entirely vertical. These results apply to the situation where the capacitative reactance is far greater than R_∞; thus, arc 3 is too small to appear on this scale. Here again curvature appears, even in a completely blocking situation when $\pi_m^{\pm 1} \gg 1$. It is therefore dangerous, even when complete blocking can in fact be assured, to ascribe observed curvature only to electrode roughness.

The reason the curves of Fig. 14 are not almost exactly vertical even in a completely blocking situation is that the exact equivalent circuit of Fig. 2(a) leads to C_g in parallel with the series combination of C_i, R_i, and R_∞. In this frequency range, where $\Omega < 0.1$, $C_{iN} \cong C_{iN0}$ for complete blocking, virtually independent of frequency. But for $\pi_m^{\pm 1} \gg 1$, R_{iN} is far greater than unity and is frequency dependent. It is the presence of this "interface" resistance R_{iN} in series with $C_{iN0} = r - 1 \cong M \cong C_{dN}$ that causes the departure from verticality. For the present situation at $\Omega = 10^{-8}$, $R_{iN} \cong 2.98\times10^2$, 1.09×10^3, and 3.31×10^3 for $\pi_g = 0.25$, 1, and 4, respectively. The real part of Z_{TN} is thus entirely dominated by R_{iN}. Now R_{iN} increases from a very small value much less than unity at $\Omega \gtrsim 0.1$ to R_{iN0} as $\Omega \to 0$. In the frequency regions covered by the curves of Fig. 14, $1 \ll R_{iN} \ll R_{iN0}$, but at constant Ω R_{iN} increases as R_{iN0} increases. Further, it turns out that for $\pi_m^{\pm 1} \gg 1$, so that $a \gg 1$, R_{iN0} is essentially equal to a. Thus, the larger the ratio of mobilities, the larger a, and the larger the departure from verticality one may expect in a completely blocking situation. In this connection it is worth mentioning that the solid electrolytes investigated by Armstrong *et al.*[17] are very likely to have a large mobility ratio.

Although the curves of Fig. 14 are shown as turning

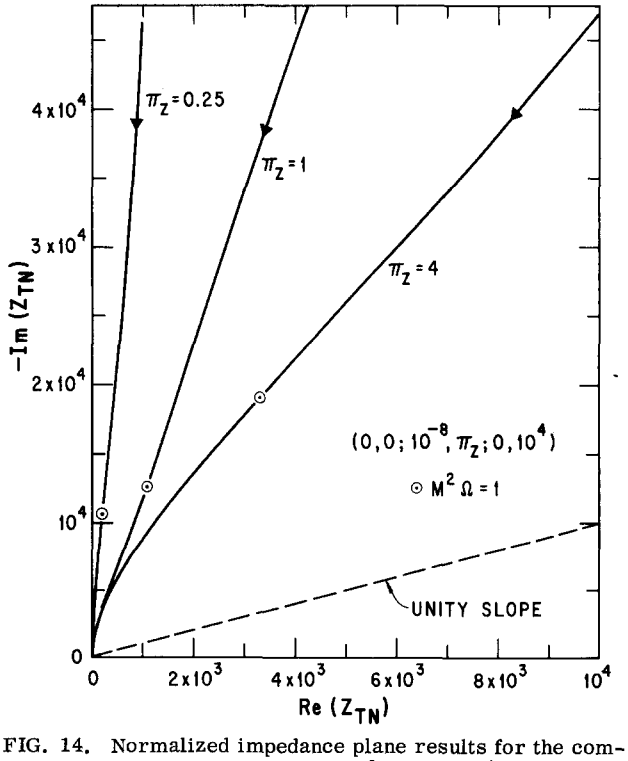

FIG. 14. Normalized impedance plane results for the completely blocking situation (0, 0; 10^{-8}, π_g; 0, 10^4).

TABLE IV. Components of Z_{TN} at $\Omega = 10^{-8}$ for $(0, r_n; 10^{-8}, 1; 0, 10^4)$.

r_n	$\mathrm{Re}(Z_{TN})$	$-\mathrm{Im}(Z_{TN})$
0	1.085×10^3	1.273×10^4
2×10^2	1.124×10^3	1.276×10^4
2×10^4	3.151×10^3	1.256×10^4
∞	3.629×10^3	1.142×10^4

over to the right, such behavior does not continue indefinitely in the completely blocking case as Ω gets smaller. Clearly when $\Omega < 2.5\ (bM^2)^{-1}$, so that $R_{iN} \cong R_{iN0}$, the curves will again approach verticality, with $\mathrm{Re}(Z_{TN}) \cong 1 + R_{iN0}$.

Finally, it is worth pointing out that the curves of Fig. 14 are primarily controlled by the small value of π_m present, not by whether r_n is zero or not. When π_m is sufficiently small, the reaction rate of the negative charge carriers is largely irrelevant because their mobility is so small relative to that of the positive carriers. This conclusion is quantified by the results of Table IV taken at $\Omega = 10^{-8}$. Here, all values of $\mathrm{Re}(Z_{TN})$ given are essentially just R_{iN} values. Not until $r_n \gtrsim 2\times10^4$ does $\mathrm{Re}(Z_{TN})$ depart appreciably from its $r_n = 0$ value. These results show that in the frequency range covered by Fig. 14 it will again be virtually impossible to distinguish between a $(0, 0)$ and a $(0, r_n)$ situation unless $r_n \gtrsim M$. Otherwise, good distinction will be possible only if frequency response measurements can be carried to low enough frequencies to show up the difference between $(0, 0)$ curves, which must eventually turn more vertical, and $(0. r_n)$ curves, which must eventually curve over to the real axis.

APPENDIX

A. Eigenvalues

Two eigenvalues, θ_1^2 and θ_2^2, enter importantly into the exact solution of the present problem.[1] Their use has been avoided in the simplified formulas of the main text but cannot be sidestepped in the more complex expressions derived subsequently. Thus, before discussing more accurate expressions for Y_{1N} and Y_{2N}, the eigenvalues need some examination.

In the general case, the full eigenvalue expressions are[1]

$$\theta_+^2 \equiv \theta_1^2 \equiv 0.5\{1 + i\Omega d + [1 + 2i\Omega(a-b) - (\Omega c)^2]^{1/2}\} \quad \text{(A1)}$$

and

$$\theta_-^2 \equiv \theta_2^2 \equiv 0.5\{1 + i\Omega d - [1 + 2i\Omega(a-b) - (\Omega c)^2]^{1/2}\}. \quad \text{(A2)}$$

Here

$$d \equiv a + b \equiv (\delta_n/\epsilon_n) + (\delta_p/\epsilon_p);$$

$$a \equiv (\delta_n^2/\epsilon_n) + (\delta_p^2/\epsilon_p);$$

$$b \equiv \delta_n\delta_p/\epsilon_n\epsilon_p;$$

and

$$c \equiv (\delta_n/\epsilon_n) - (\delta_p/\epsilon_p \equiv (\delta_p/\epsilon_n)(\pi_z - \pi_m).$$

It follows that

$$(a-b) \equiv (\delta_n - \delta_p)c \equiv (\delta_p^2/\epsilon_n)(\pi_z - 1)(\pi_z - \pi_m).$$

When $\pi_m = \pi_z$, $a = b = 1$, $c = 0$, and $d = 2$. Further when $\pi_z = 1$, $a = b = (4\epsilon_n\epsilon_p)^{-1} = (\pi_m + 2 + \pi_m^{-1})/4$. This quantity will be very large when $\pi_m \ll 1$ or $\pi_m \gg 1$.

Two approximate expansions of (A1) and (A2) are often useful. When $\Omega(a-1) \ll 1$, one finds

$$\theta_1^2 \cong 1 + i\Omega a \quad \text{(A3)}$$

and

$$\theta_2^2 \cong i\Omega b. \quad \text{(A4)}$$

These results are exact for all Ω in the special $c = 0$ case where $\pi_m = \pi_z$ and $a = b = 1$.

Interesting things happen to $\theta_\pm^2$ in the $\pi_m \neq \pi_z$ case when $(\Omega c)^2 = 1$ and when $(\Omega c)^2 \gg 1$. When $\pi_z = 1$ as well, the square root term disappears at the $(\Omega c)^2 = 1$ point and $\theta_\pm^2 = 0.5 + i\Omega a = 0.5 + 0.5i(|\epsilon_p - \epsilon_n|)^{-1}$. The branch point at $(\Omega c)^2 = 1$ in this $\pi_z = 1$ case leads to possible ambiguity in the assignment of θ_+^2 and θ_-^2 to θ_1^2 and θ_2^2 for $\Omega \geq |c|^{-1}$. Such ambiguity is of no consequence in the exact solution since it is indifferent to the assignment. Our present inexact solutions may not be, however, and it is thus important to choose that pairing that leads to simplest and most accurate results in the region $(\Omega c)^2 \geq 1$.

When $(\Omega c)^2 \gg 1$, one can readily expand the square-root terms in the exact solution and obtain first-order expansions for $\theta_\pm^2$. For this case, I have made the following θ_1^2, θ_2^2 choices for the expansions:

$$\left.\begin{aligned}\theta_1^2 &\cong \delta_n + i\Omega(\delta_n/\epsilon_n)\cdots\\ \theta_2^2 &\cong \delta_p + i\Omega(\delta_p/\epsilon_n)\cdots\end{aligned}\right\} \quad (\Omega c)^2 \gg 1,\ \pi_m > \pi_z \quad \text{(A5), (A6)}$$

and

$$\left.\begin{aligned}\theta_1^2 &\cong \delta_p + i\Omega(\delta_p/\epsilon_p)\cdots\\ \theta_2^2 &\cong \delta_n + i\Omega(\delta_n/\epsilon_n)\cdots\end{aligned}\right\} \quad (\Omega c)^2 \gg 1,\ \pi_m < \pi_z. \quad \text{(A7), (A8)}$$

Note that the sign of $c \equiv (\delta_p/\epsilon_n)(\pi_z - \pi_m)$ depends directly on that of $(\pi_z - \pi_m)$. The above choices ensure that under all π_m, π_z conditions $\mathrm{Re}(\theta_1^2) \gg \mathrm{Im}(\theta_1^2)$ for sufficiently small Ω, as is also the case for θ_1^2 when $(\Omega c)^2 \ll 1$. The present expansion is of course invalid when $\pi_m = \pi_z$ and $c \equiv 0$.

In the exact theory,[1] several functions of θ_1 and θ_2 appear. Those that will be used in the admittance formulas of the Appendix are

$$\gamma_j \equiv (M\theta_j)\coth(M\theta_j) \quad \text{(A9)}$$

and

$$t_j \equiv \gamma_j - 1, \quad \text{(A10)}$$

where $j = 1$ and 2. When $\pi_m = \pi_z \equiv \pi_e$, $\gamma_1 = (Mp)\coth(Mp)$ and $\gamma_2 = (iM^2\Omega)^{1/2}\coth(iM^2\Omega)^{1/2}$.

B. Exact and approximate admittance results for $\pi_m = \pi_z \equiv \pi_e$

First consider the $r_p = r_n \equiv r_e$ situation. The full solution[1] yields in this high symmetry case the simple exact result

$$Y_{iN} = i\Omega p^{-2} g_e^{-2} t_1. \quad \text{(A11)}$$

When this expression and $R_{EN} = g_e$ are substituted into

Eq. (2) one obtains

$$Y_{12N} = Y_{2N} = p^2[\, p^2(r_e/2) + i\Omega\gamma_1], \tag{A12}$$

in agreement with an earlier result[4] for $r_e = 0$.

Notice that Eq. (A12), and hence Z_{TN}, is wholly independent of π_e in this $(r_e, r_e;\ \pi_e, \pi_e;\ 0, M)$ case. It follows from (A12) that $G_{2N0} = (r_e/2)$ and $C_{2N0} = (r + r_e)$. The parallel quantities G_{PN0} and C_{PN0} thus become $G_{PN0} = [1 + (2/r_e)]^{-1}$ and $C_{PN0} = 1 + g_e^{-2}(r - 1)$, quite different from the arc 2 quantities. When $r \gg r_e$, the quantity Ω_{2M} is closely given by the solution of the approximate equation $\Omega(r + r_e) = 0.5\ (r_e - 3\Omega^2 r)$. Then

$$\Omega_{2M} \cong [r_e - (3r_e^2/4r)]/2(r + r_e) \simeq r_e/2r\,.$$

It follows that

$$\rho_{2N} \cong [r_e - (3r_e^2/4r)]^{-1} \simeq r_e^{-1}\,.$$

The other situation where a simple exact result can be derived is $(r_p, \infty;\ \pi_e, \pi_e;\ 0, M)$. Earlier results[1,2,4] and Eq. (2) yield

$$Y_{12N} = Y_{1N} = p^2\{\, p^2[\pi_e\gamma_2 + (r_p/2\epsilon_p)] + i\Omega\gamma_1 \}. \tag{A13}$$

It follows that $G_{1N0} = [\pi_e + (r_p/2\epsilon_p)]$ and $C_{1N0} = \pi_e[(M^2/3) + 2] + [r + (r_p/\epsilon_p)]$. In addition, $G_{PN0} = G_{DN} = \epsilon_n + \epsilon_p[1 + (2/r_p)]^{-1}$ and $C_{PN0} = 1 + g_p^{-2}[(\delta_n\delta_p M^2/3) + \delta_p^2(r - 1)]$, where here $\epsilon_n = \delta_n$, $\epsilon_p = \delta_p$. Notice that Eq. (16) does not reduce to (A13) in the $(0, \infty;\ \pi_e, \pi_e;\ 0, M)$ case because the difference between p^2 and unity has been neglected in (16), as has the term $i\Omega\gamma_1$, valid when $M \gg 10^2$.

It is natural to ask how well the present Y_{1N} and Y_{2N} results, which are exact separately, work together in the $(0, r_n;\ \pi_e, \pi_e;\ 0, M)$ case. The Z_{TN} calculated using Eqs. (A12) and (A13) together is exact when $r_n = \infty$ but only valid when $r_n = 0$ if Y_{1N} is then taken infinite. Some intermediate r_n results for $M = 10^5$ have been examined over the Ω range $10^{-10}(10)1$, i.e., at decade intervals in Ω. For $\pi_e = 1$, it is found that for an r_n range of $0.1(10)10^8$, $|P_R|$ is generally less than 0.1%, reaching 0.2% at $r_n = 0.1$ and remaining below 10^{-6}% for $r_n \geq 10^8$. On the other hand, $|P_I|_{\max}$ may be appreciably larger. For $r_n = 10^8$, $|P_I|_{\max}$ is less than 2×10^{-4}%. It reaches about 4% at $r_n = 100$ and is down to about 2% at $r_n = 1$. Over most of the Ω range, $|P_I|$ is less than 0.1%, however, and the regions where it is considerably larger coincide with those where $-\mathrm{Im}(Z_{TN})$ is near a relative minimum. Such regions, where $-\mathrm{Im}(Z_{TN}) < 0.1$, are of small importance in the overall picture anyway and probably are where experimental measurements for $-\mathrm{Im}(Z_{TN})$ tend to be least accurate. Similar results to the above are found for $(0, 10^4;\ 0.25, 0.25;\ 0, 10^5)$, although $|P_I|_{\max}$ reaches about 5% for this case.

These general results are sufficiently favorable to suggest that a useful plan of attack when $\pi_m \neq \pi_z$ is to find adequate expressions for Y_{1N} in the (r_p, ∞) situation and for Y_{2N} for (r_e, r_e) and then combine them as above for (r_p, r_n), or at least for the case of most interest, $(0, r_n)$. This course of action is followed below.

C. Approximate admittance results for $(r_e, r_e\ ;\ \pi_m, \pi_z\ ;\ 0, M)$

In this more complicated situation, the exact theory leads to no simple expression for Y_{2N}. There are certain conditions that an approximate formula should satisfy, however, which may be helpful in synthesizing a useful result. First, it should be invariant under the transformation $(\pi_m, \pi_z) \to (\pi_m^{-1}, \pi_z^{-1})$. Second, it should lead to the exact G_{2N0} and C_{2N0} results. Unfortunately, this second condition is not particularly helpful here since it turns out that G_{2N0} and C_{2N0} are the same for the general (π_m, π_z) case as they are for $\pi_m = \pi_z \equiv \pi_e$. Some help comes, however, from ensuring that terms in Ω^2 are correct as $\Omega \to 0$, especially when $r_e = 0$.

The synthesis begins by adding plausible terms to (A12) which nevertheless allow the results to still reduce essentially to (A12) when $\pi_m = \pi_z \equiv \pi_e$. Then by examining the numerical differences between the approximate Y_{2N} expression, here denoted as Y_{2N1}, and the exact Y_{2N} as a function of Ω, modifications to reduce the differences can be made. The best result obtained so far is

$$Y_{2N} \cong Y_{2N1} = p^2[(p^2/2)(\epsilon_n r_n + \epsilon_p r_p) + i\Omega + p^2 Q], \tag{A14}$$

where

$$Q \equiv \left(\frac{i\Omega t_1}{1 + i\Omega(1 + \gamma_2^{-1}\{ g_n^{-2}(r-1)R'_{iN0} - 1 + [ar/2(r-1)]\})} \right) \tag{A15}$$

and

$$R'_{iN0} \equiv g_n\left[(a-1) + \left(\frac{ag_n}{r-1}\right)\left(1 + \frac{(M^2\mathrm{csch}^2 M - r)}{2(r-1)}\right)\right]. \tag{A16}$$

Note that the full expressions for θ_1 and θ_2 must be used here in calculating t_1 and γ_2. The γ_2^{-1} term in the denominator corrects for terms in Y_{2N} of order $\Omega^{3/2}$.

This approximation for Y_{2N}, which holds well down to $M \sim 1$ when it is a good approximation for large M, could be further improved, but only at the cost of considerable additional complexity. I have written the expression for Y_{2N1} in terms of r_n and r_p in this $r_n = r_p \equiv r_e$ case so that it may be used, to whatever degree it is applicable, in the $(0, r_n)$ case and possibly even in some (r_p, r_n) cases with $r_p \ll r_n$ as well, situations where Z_{TN} will involve Z_{1N}, Z_{2N}, and Z_{3N} when $r_n, r_p \neq \infty$. The expression for R'_{iN0} above is just the exact[1] R_{iN0} in the $r_n = r_p = r_e$ case when g_n is set equal to g_e.

Equations (A14)–(A16) lead to Eqs. (5)–(7) in the text for $\Omega \to 0$. Whenever the text equations are reasonably good approximations for $\Omega \ll \Omega_S$, the present results generally yield better approximations over the entire Ω range of interest: $0 \leq \Omega \lesssim 1$. Very considerable improvement generally occurs for $r_p = r_n \equiv r_e$ cases, less for others. Some comparisons have already been presented in Table II. None of the equations is really adequate in the transition region where $\pi_m^{\pm 1} \gtrsim 100$ and yet is not large enough to lead to plateau conditions. A simple equation for the plateau region itself has already been discussed, and a somewhat more accurate result is

$$Y_{2N} = Y_{2SN} \cong [(\epsilon_n r_n + \epsilon_p r_p)(0.5 + i\Omega) + (i\Omega - 1.5\Omega^2)\gamma_1], \tag{A17}$$

where γ_1 here involves the θ_1 of Eqs. (A5) and (A7). Thus, Eq. (A17) applies only when $(\Omega c)^2 > 1$, a condition consistent with the plateau requirement $\Omega \gg \Omega_S = (a-1)^{-1}$.

D. Approximate admittance results for $(r_p, \infty; \pi_m, \pi_z; 0, M)$

To derive an approximate relation for Y_{1N} in this case, one may first start with Eq. (A13) and generalize it to yield the correct G_{1N0} and C_{1N0} results while still requiring it to reduce to (A13) when $\pi_m = \pi_z \equiv \pi_e$. The exact results[1] readily lead to

$$G_{1N0} = \pi_m + (r_p/2\epsilon_p) \tag{A18}$$

and

$$C_{1N0} = [(2g_p/\epsilon_p) - 1] + \epsilon_p^{-2}[(\delta_n\delta_p M^2/3) + \delta_p^2(\gamma - 1)], \tag{A19}$$

where $[(2g_p/\epsilon_p) - 1]$ may also be written as $[(r_p/\epsilon_p) + 2\pi_m + 1] = [(r_p/\epsilon_p) + \pi_m + \epsilon_p^{-1}]$. The corresponding components of Y_{TN} are $G_{PN0} = G_{DN} = 1 - (\epsilon_p/g_p) = g_p^{-1}\{\epsilon_n + (r_n/2)\}$, and $C_{PN0} = 1 + (\delta_p\delta_n M^2/3g_p^2) + [\delta_p^2(\gamma - 1)/g_p^2]$.

The above procedure leads to a result which is still incorrect to order $\Omega^{3/2}$, though correct to order Ω. Numerical experimentation using the exact solution allows one to establish the form of the needed $\Omega^{3/2}$ term. The result is the still approximate expression

$$Y_{1N} \cong Y_{1N1} = p^2\{(p^2 r_p/2\epsilon_p) + p^2\pi_m\gamma_2(1 + i\Omega c_1) + i\Omega[(\delta_p/\epsilon_p)^2(\gamma_1 - 1) + 1 - p^2\pi_m c_1]\}, \tag{A20}$$

where

$$c_1 = (c/2)[(\pi_m\pi_z + 3)/(\pi_m\pi_z + 1)]. \tag{A21}$$

Although it would be possible to correct this expression to order Ω^2, the added complexity is unnecessary for $M \gtrsim 100$ since by the time incorrect Ω^2 terms become important, $|Z_{1N}| \ll |Z_{3N}|$. The above approximation does not apply very well in the plateau region where $\Omega \gg \Omega_S$. An approximate expression for this region is

$$Y_{1N} = Y_{1SN} \cong [(r_p/2\epsilon_p) + (i\Omega - 1.5\Omega^2)\gamma_1], \tag{A22}$$

where γ_1 again involves the θ_1 of Eqs. (A5) and (A7).

Equation (A20) is exact for $(r_p, \infty; \pi_e, \pi_e; 0, M)$. Some idea of its accuracy for $r_p = 0, r_n \cong \infty$ and $\pi_m \neq \pi_z$ can be formed from the following results. For $M = 10^5$, $\pi_z = 1$, and $1 \leq \pi_m \leq 10^4$, the maximum value of $|P_I|$ found is about 3×10^{-4}, with $|P_R|_{\max}$ much smaller. $|P_I|$ does not increase in the region $2 \leq \pi_m \leq 10^4$. On the other hand, for $\pi_z = 1$ and $10^{-4} \leq \pi_m \leq 1$, the error increases as π_m decreases. Again, it is principally in P_I and reaches a magnitude of about 1% by $\pi_m = 10^{-2}$ and 60% by $\pi_m = 10^{-4}$. It should be added that such maximum values of $|P_I|$ are generally isolated and occur near $\Omega \sim 10^{-2}$, where $-\mathrm{Im}(Z_{TN})$ is very small. Over most of the range of Ω, $|P_R|$ and $|P_I|$ are usually well below 0.1%.

In the $\pi_m = 1$, $\pi_z \lesssim 1$ situation, results are somewhat different. Again the maximum error shows up in $|P_I|$. Within the range $0.25 \leq \pi_z \leq 4$, $|P_I|_{\max}$ is less than 10^{-3}%. Even in the larger range $10^{-4} \leq \pi_z \leq 10^4$ (important for extrinsic conditions when π_z is re-interpreted) $|P_I|_{\max}$ remains less than 3×10^{-2}%. When $\pi_m = \pi_z^{-1}$, on the other hand, $|P_I|_{\max}$ remains less than 10^{-3}% for $1 \leq \pi_m \leq 10^3$. As might be expected from the above results, it increases as π_m decreases. It reaches about 1% by $\pi_m = 10^{-2}$ and 75% by $\pi_m = 10^{-3}$. Again such a value as 75% is an isolated peak; over most of the Ω range the formula yields $|P_R|$ and $|P_I|$ values less than 0.1% for $\pi_m = 10^{-3}$.

Let us continue to consider only the $r_p = 0, r_n = \infty$ situation and investigate the approximate Warburg response region following from Eq. (A20) when $b^{-1} < M^{-1}$. Now this region falls in the range $10(bM^2)^{-1} < \Omega < b^{-1}$, which, for the $\pi_m \ll 1$ case of interest, becomes $40\pi_m M^{-2} < \Omega < 4\pi_m$ when $\pi_z = 1$ as well. Then, for this region we may take $p^2 \cong 1$ and rewrite (A20) symbolically as

$$Y_{1N1} \cong e_0\Omega^{1/2} + e_1\Omega + e_2\Omega^{3/2}. \tag{A23}$$

It follows that $e_0 \cong \pi_m M\sqrt{ib}$ and $e_1 \cong i[(\delta_p/\epsilon_p)^2(\gamma - 1) + 1 - \pi_m c_1] \cong i(\delta_p/\epsilon_p)^2(\gamma - 1)$. On taking $(\gamma - 1) \cong M$, one finds that the ratio $|e_0\Omega^{1/2}|/|e_1\Omega|$ becomes approximately $(\epsilon_n\epsilon_p/\delta_p^2)(b/\Omega)^{1/2}$. For $\Omega = b^{-1}$, this reduces to just π_z. Thus, in the main part of the Warburg region where $\Omega \ll b^{-1}$, the ratio will be much greater than unity. Further, the third term on the right will also be much less in magnitude than the first term.

Under the above conditions, one can immediately calculate $Z_{1N1} \equiv Y_{1N1}^{-1}$ by series expansion and obtain

$$Z_{1N1} \cong (e_0\Omega^{1/2})^{-1}[1 - (e_1/e_0)\Omega^{1/2} - (e_2/e_0)\Omega \cdots]. \tag{A24}$$

Now $(e_0\Omega^{1/2})^{-1} = Z_{WN} \equiv A(1 - i)/\sqrt{\Omega}$, an exact normalized Warburg impedance, with A defined in Eq. (20). On neglecting the e_2 term, one obtains

$$Z_{1N1} \simeq Z_{WN} - (e_1/e_0^2) \equiv Z_{WN} + R_{C1N}, \tag{A25}$$

where

$$R_{C1N} \equiv -(\delta_p/\epsilon_p\pi_m M)^2(\gamma - 1)/b \cong -(\pi_m\pi_z M)^{-1}. \tag{A26}$$

Thus, to this order of approximation, Z_1 shows exact Warburg response plus a negative, frequency-independent resistence R_{C1}.

E. Approximate admittance results for $(r_p, r_n; \pi_m, \pi_z; 0, M)$

Here, we shall primarily consider the $r_p = 0$ situation but with some investigation of the utility of the results when $r_p < r_n$. The plan of approach is to combine the approximate results given in Eqs. (A14) and (A20), or (A17) and (A22) for the plateau region. Since Z_{1N} should be zero when $r_p = r_n$ and $s \equiv r_p/r_n$ is unity, it turns out that the Y_{1N}'s given in Eqs. (A20) and (A22) should be multiplied by $(1 - s)^{-2}$ in order to ensure that this is the case. Although the $(1 - s)^{-2}$ term will be shown to be correct for $s = 0$ and 1, it is only an approximation otherwise.

We may now write

$$Z_{TN} \cong Z_{TN1} \equiv Z_{1N1} + Z_{2N1} + Z_{3N}, \tag{A27}$$

where Z_{2N1} is formed from the Y_{2N1} of Eq. (A14) and $Z_{1N1} = Y_{1N1}^{-1}(1 - s)^2$, with Y_{1N1} from Eq. (A20). The result should be most applicable when either $r_p \cong r_n$ or $0 \leq r_p \ll r_n$.

Let us now investigate how Z_{TN10} differs from $Z_{TN0} = R_{DN}$. Analysis shows that

$$Z_{TN0} \equiv 1 + [2/(\epsilon_n r_n + \epsilon_p r_p)] + H_0^{-1}, \tag{A28}$$

where

$$H_0 \equiv \{\pi_m + (r_p/2\epsilon_p) + s[2 + (r_p/2\epsilon_n) + \pi_m^{-1}s]\}(1 - s)^{-2}. \tag{A29}$$

But Eq. (A27) leads to

$$Z_{TN0} = 1 + [2/(\epsilon_n r_n + \epsilon_p r_p)] + H_1^{-1}\,, \tag{A30}$$

where

$$H_1 = [\pi_m + (r_p/2\epsilon_p)](1-s)^{-2}\,. \tag{A31}$$

Comparison of (A29) and (A31) shows that they yield the same results for $s=0$ and 1 but that the s term in (A29) has been omitted for simplicity from (A31). Even when $r_p \sim 0$, the s term will only be negligible when $s \ll \pi_m$.

The accuracy of Eq. (A27) in the general $(r_p, r_n;\ \pi_m,\ \pi_s;\ 0, M)$ case is illustrated by many of the results of Table II. There is some slight tendency for errors to increase as r_n decreases in the range $r_n \ll M$. For $r_n \gtrsim M$, errors are generally quite negligible. For $M = 10^5$, $r_n = 10^3$, and $\pi_s = 1$, $|P_I|_{\max}$ increases with increase in $\pi_m^{\pm 1}$. At $\pi_m = 10^3$ and $\pi_m = 10^{-1}$ it is under 8%. For $M = 10^5$, $r_n = 0.1$, and $\pi_m = 0.1$, it is under 12%. As usual, the major percentage errors occur in P_I rather than P_R, usually because $|\mathrm{Im}(Z_{TN})| \ll \mathrm{Re}(Z_{TN})$. All major errors here arise not so much from errors in the individual (r_e, r_e) Z_{2N} and (r_p, ∞) Z_{1N} expressions but because of the simple way they are combined in the present (r_p, r_n) situation.

Finally, let us examine response in the Warburg region, restricting attention to the $r_p = 0$, $0 < r_n \leq \infty$ situation. In the Warburg region, where $\Omega \ll 1$ and $\Omega \ll \Omega_{2M}$, $Z_{3N} \cong Z_{3N0} = 1$ and $Z_{2N} \cong Z_{2N0} = (P_{2N} - 1)$. Then the approximate equivalent circuit of Fig. 15(a) reduces to that of Fig. 15(b), where pure Warburg elements are enclosed by dashes. On using these results and Eq. (A25) as well, one may write

$$Z_{TN} \cong Z_{WN} + R_{C1N} + P_{2N} = (i\Omega C_{WSN})^{-1} + R_{SN}\,, \tag{A32}$$

where

$$C_{WSN} \equiv (A\Omega^{1/2})^{-1}\,, \tag{A33}$$

$$R_{SN} \equiv R_{WSN} + R_{RN}\,, \tag{A34}$$

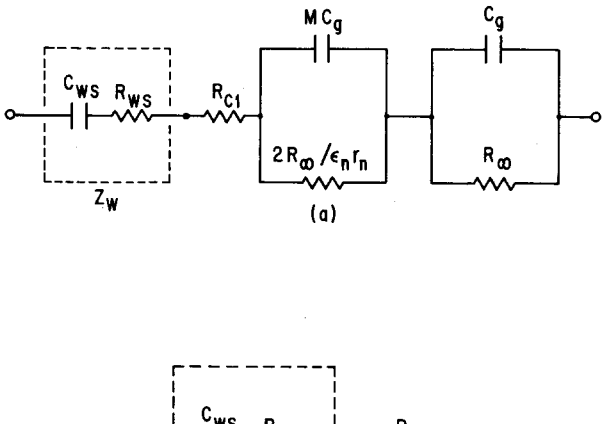

FIG. 15. (a) Approximate series-parallel equivalent circuit in the Warburg response region. (b) Simplified approximate equivalent circuit in the Warburg region. Ideal Warburg elements enclosed in dashed box.

$$R_{WSN} \equiv (A/\Omega^{1/2})\,, \tag{A35}$$

and

$$R_{RN} \equiv R_{C1N} + P_{2N} = 1 + (2/\epsilon_n r_n) - (\pi_m \pi_s M)^{-1}\,. \tag{A36}$$

Thus in this region Z_{TN} is approximately made up of an exact Warburg impedance $Z_{WN} \equiv R_{WSN} + (i\Omega C_{WSN})^{-1}$ and a frequency-independent resistance R_{RN}. Such response is frequently found experimentally.[2]

The above results lead to

$$[\mathrm{Re}(Z_{TN}) - R_{RN}] \cong -\mathrm{Im}(Z_{TN}) \cong A\Omega^{-1/2}\,. \tag{A37}$$

Therefore, plotting $-\mathrm{Im}(Z_{TN})$ *versus* $[\mathrm{Re}(Z_{TN}) - R_{RN}]$ in the impedance plane should yield a straight line at a 45° slope. We shall use this condition below as a test of Warburg response. Further, note that if R_{RN} or R_R is initially unknown, it may be determined from the data by selecting the value subtracted from $\mathrm{Re}(Z_{TN})$ which yields the best and straightest approximation to a straight line at 45°. Then the present somewhat more accurate approach may be used in the same way as Eq. (22) of the body of this paper to estimate the value of π_m.

It is interesting that $(R_{RN} - 1)$ or even R_{RN} may be zero for certain values of π_m, π_s, r_n, and M. Note that $(R_{RN} - 1)$ corresponds to $(R_R - R_\infty)$, the usual subtraction of the bulk resistance from the total frequency-independent resistance. Further $(R_{RN} - 1)$ is very nearly the same under wide conditions as the normalized resistance R_{CSN} which appeared in the earlier work.[2] When $r_n \gg 2$, it turns out that $(R_{RN} - 1)$ and $\epsilon_p^2 R_{CSN}$ are virtually identical. In the $\pi_m \ll 1$ case of principal interest, $\epsilon_p \cong 1$. The difference between the two quantities occurs because they appear in different equivalent circuits. When $\pi_m \ll 1$, $(R_{RN} - 1)$ is zero when $r_n = 2\pi_s M$.

A more exact Warburg region condition may be derived by requiring that

$$\beta \equiv \tan^{-1}\{-\mathrm{Im}(Z_{TN})/[\mathrm{Re}(Z_{TN}) - R_{RN}]\} \tag{A38}$$

be $(45° \pm 2°)$. It actually turns out that $(45° - \sim 0°)$ and $(45° + 2°)$ are the limits of interest. Then on the basis of numerous numerical results one finds that β reaches $\approx 45°$ by $\Omega \gtrsim 25(bM^2)^{-1}$ and remains less than $\sim 47°$ until $\Omega \sim I_1$. Here I_1 is the smallest of $I_a \equiv (10M)^{-1}$, $I_b \equiv (10b)^{-1}$, and $I_c \equiv r_n/(800bM)$. It is always necessary for $\Omega \lesssim M^{-1}$ for Warburg response to occur. Thus, Warburg response, as defined by $\beta \simeq 45°$, occurs when

$$25(bM^2)^{-1} \lesssim \Omega \lesssim I_1\,. \tag{A39}$$

When $\pi_m \ll 1$, $\pi_s = 1$, $r_n < 80M$, and $r_n < 80b$, the conditions become

$$100\pi_m M^{-2} \lesssim \Omega \lesssim r_n \pi_m / 200M\,. \tag{A40}$$

Since $\Omega_{2M} = \epsilon_n r_n / 2M \cong r_n \pi_m / 2M$ for $\pi_m \ll 1$, condition (A40) requires that $\Omega \ll \Omega_{2M}$ for Warburg behavior to appear, as initially stated. Finally, note that no such response shows up when $r_n M \lesssim 2 \times 10^4$. Under such conditions Z_{2N} rather than Z_{1N} dominates Z_{TN}.

Finally for completeness, since $C_{PN0} \equiv 1 + C_{iN0}$, it is worthwhile to give the exact expression for C_{iN0} in the present general case. It is[1,2]

$$C_{iN0} = (g_p g_n)^{-2}[(\delta_n \delta_p M^2/3)(g_p - g_n)^2 + (\gamma - 1) g_s^2]\,, \tag{A41}$$

where $g_s \equiv g_p \delta_n + g_n \delta_p$. Some special results for R_{tN0} are given elsewhere.[1]

*Present address: Department of Physics and Astronomy, University of North Carolina, Chapel Hill, NC 27514.

[1]J. R. Macdonald, J. Chem. Phys. 58, 4982 (1973); 60, 343 (1974).
[2]J. R. Macdonald, J. Electroanal. Chem. 53, 1 (1974).
[3]K. S. Cole and R. H. Cole, J. Chem. Phys. 9, 341 (1941).
[4]J. R. Macdonald, J. Electroanal. Chem. 32, 317 (1971).
[5]J. Volger, Progr. Semicond. 4, 207 (1960).
[6]J. R. Macdonald, J. Chem. Phys. 22, 1317 (1954).
[7]H. R. Thirsk and J. A. Harrison, *A Guide to the Study of Electrode Kinetics* (Academic, London, 1972), p. 80.
[8]D. R. Powell and J. R. Macdonald, Comput. J. 15, 148 (1972); 16, 51 (1973). A Fortran program listing is available from the authors. See also, H. I. Britt and R. H. Luecke, Technometrics 15, 233 (1973).
[9]K. S. Cole, *Membranes, Ions, and Impulses* (University of California Press, Berkeley, 1968), pp. 26, 38, 176.
[10]R. P. Buck (private communication).
[11]R. P. Buck and I. Krull, J. Electroanal. Chem. 18, 387 (1968).
[12]M. J. D. Brand and G. A. Rechnitz, Anal. Chem. 41, 1185 (1969).
[13]N. G. Bukun, E. A. Ukshe, and V. V. Evtushenko, Elektrokhimiya 9, 406 (1973).
[14]R. D. Armstrong, T. Dickinson, and P. M. Willis, Electroanal. Chem. Interfacial Electrochem. 48, 47 (1973).
[15]J. H. Sluyters, Rec. Trav. Chim. 79, 1092 (1960).
[16]J. R. Macdonald, J. Appl. Phys. 44, 3455 (1973); 45, 73 (1974); 45, 2343 (1974).
[17]R. D. Armstrong, T. Dickinson, and P. M. Willis, J. Electroanal. Chem. 53, 389 (1974).
[18]R. de Levie, Adv. Electrochem. 6, 329 (1967).